

A Winning Hand: Compressing Deep Networks Can Improve Out-Of-Distribution Robustness

James Diffenderfer, Brian R. Bartoldson*, Shreya Chaganti*, Jize Zhang, Bhavya Kailkhura
Lawrence Livermore National Laboratory
{diffenderfer2, bartoldson, chaganti1, zhang64, kailkhura1}@llnl.gov

Abstract

Two crucial requirements for a successful adoption of deep learning (DL) in the wild are: (1) robustness to distributional shifts, and (2) model compactness for achieving efficiency. Unfortunately, efforts towards simultaneously achieving Out-of-Distribution (OoD) robustness and extreme model compactness without sacrificing accuracy have mostly been unsuccessful. This raises an important question: *“Is the inability to create Compact, Accurate, and Robust Deep neural networks (CARDs) fundamental?”* To answer this question, we perform a large-scale analysis for a range of popular model compression techniques which uncovers several intriguing patterns. Notably, in contrast to traditional pruning approaches (e.g., fine tuning and gradual magnitude pruning), we find that “lottery ticket-style” pruning approaches can surprisingly be used to create high performing CARDs. Specifically, we are able to create extremely compact CARDs that are dramatically more robust than their significantly larger and full-precision counterparts while matching (or beating) their test accuracy, simply by pruning and/or quantizing. To better understand these differences, we perform sensitivity analysis in the Fourier domain for CARDs trained using different data augmentation methods. Motivated by our analysis, we develop a simple domain-adaptive test-time ensembling approach (CARD-Deck) that uses a gating module to dynamically select an appropriate CARD from the CARD-Deck for each test sample based on their spectral-similarity with test samples. By leveraging complementary frequency biases of different compressed models, the proposed approach builds a “winning hand” of CARDs that establishes a new state-of-the-art on CIFAR-10-C accuracies (i.e., 96.8% *clean* and 92.75% *robust*) with dramatically better memory usage than existing non-compressed baselines. We also present theoretical evidences supporting our empirical findings.

1 Introduction

Deep Neural Networks (DNNs) have achieved unprecedented success in a wide range of applications due to their remarkably high accuracy [13]. However, these advances predominantly come from significant growth in the model size due to massive overparameterization. Furthermore, these highly overparameterized models are known to be susceptible to the out-of-distribution (OoD) shifts encountered during their deployment in the wild [3]. This resource-inefficiency and OoD brittleness of state-of-the-art (SOTA) DNNs severely limits the potential applications DL can make an impact on. For example, consider the real-world use case of the “Mars rover mission” that uses laser-induced breakdown spectroscopy (LIBS) to search for indicators of microbial life. It is well accepted that endowing the Perseverance rover with DNNs to analyze high-dimensional and complex LIBS spectra offers a huge potential to make scientific breakthroughs [1]. Yet, such an effort is non-existent because: 1) as these devices are battery operated, the model has to be lightweight so it consumes

*equal contribution

less memory with reduced power consumption, and 2) the model must be able to efficiently handle domain shifts in spectral data caused by environmental or sensor noise. Both of these requirements are not specific only to the aforementioned planetary exploration use case but arise in virtually any resource-limited application using machine learning (ML) in the wild. The fact that existing SOTA DNNs do not satisfy *model compactness* and *OoD robustness* requirements is holding us back from leveraging the advances in DL to enable game changing scientific discoveries.

In this paper, we are driven by two questions around this crucial problem. **Q1.** *Can we show the existence of compact, accurate, and robust DNNs (CARDs)?* **Q2.** *If yes, can we develop efficient algorithms to design CARDs that match (or beat) the performance of SOTA robust-DNNs?*

There have been some recent successes in addressing each of the challenges CARDs present in isolation. The authors in [22, 25] developed data augmentation methods for achieving high OoD robustness without sacrificing accuracy on the clean data. The authors in [10, 7] developed pruning and quantization approaches for achieving high accuracy at extreme levels of model compression. However, efforts towards achieving model compactness, high accuracy, and OoD robustness simultaneously have mostly been unsuccessful. For example, [24] and [30] recently showed that compressed DNNs achieve accuracy as high as the original network’s, but are far more brittle when faced with OoD data. Perhaps unsurprisingly, the current solution in the robust ML community to improve the OoD robustness (and accuracy) is to increase the model size (e.g., [23, 14, 6]).

In this paper, we argue that these negative results are a byproduct of inapt compression strategies, and the inability to create CARDs is not fundamental (answering **Q1** in the affirmative). Specifically, to answer **Q1**, we perform a large-scale comparison by varying architectures, training methods, and pruning rates for a broad range of popular model compression techniques. Our empirical study uncovers several intriguing patterns. We find that in contrast to traditional pruning methods analyzed in past studies (e.g., fine tuning [16] and gradual magnitude pruning [52]), “lottery ticket-style” compression approaches [10, 40, 38, 7] can surprisingly be used to create high performing CARDs. Specifically, we are able to create extremely compact (i.e., sparse and/or binary) CARDs that are dramatically more robust compared to their significantly larger and full-precision counterparts while matching (or beating) their test accuracy. Our results are in sharp contrast to the existing observation that compression is harmful to OoD robustness. In fact, we show that compression, if done properly, improves OoD robustness. Next, we show that within a random-weight neural network, there exist CARDs which perform equally well when compared to more computationally expensive methods without ever modifying the values of the weights. Moreover, this class of models demonstrates a very peculiar behavior when using Global vs. Layerwise pruning methods. Globally pruned models are significantly more robust but less accurate than Layerwise pruned models. Finally, rewinding-based pruning methods are uniformly accurate and robust, provided a sufficient number of pruning iterations is used.

To better understand these differences and why they occur, we analyze these compressed models through the lens of Fourier sensitivity analysis in the spectral domain. We find that traditional pruning methods end up with compressed models that are highly brittle to additive noise in all but the lowest frequencies. We show that “lottery ticket-style” pruning methods generate compressed models that are more robust compared to dense models at all the frequency ranges. Note that clean (or natural) data is dominated by the power at only a few low frequencies as opposed to the OoD (or corrupted) data that is mostly mid-to-high frequency in nature. This offers the much needed explanation for the higher apparent robustness of lottery ticket-style pruning methods relative to traditional pruning methods. We perform a similar analysis with different training (or data augmentation) methods and show that these methods trade-off robustness at certain frequencies for others (“accuracy-robustness trade-off”). Our analysis highlights that model robustness on OoD data is dependent on the interaction between the frequencies the model is biased towards and the frequencies the test-time corruption is concentrated on.

Motivated by this, we propose a *spectral-similarity metric* that compares the spectral behavior of training augmentations with the spectral behavior of OoD (or corrupted) data and show that the proposed metric is a strong predictor of the corruption error. Using this metric, we develop a simple test-time domain-adaptive ensemble approach (CARD-Deck) that uses a gating module to dynamically choose an appropriate CARD for each test sample by maximizing their spectral-similarity w.r.t. the augmented training data. By leveraging the complementary frequency biases of different CARDs, the proposed test-time ensembling approach builds a “winning hand” of CARDs that establishes a new

state-of-the-art robustness (and accuracy) on the popular OoD benchmark dataset CIFAR-10-C [26] with an extremely compact ensemble (answering **Q2** in the affirmative). Finally, we present some theoretical evidences supporting our empirical findings.

Our main contributions are summarized as follows²:

- To the best of our knowledge, we present the first positive result on simultaneously achieving high accuracy and OoD robustness at extreme levels of model compression.
- Our study reveals an intriguing finding – “lottery ticket-style” pruned models are dramatically more robust compared to their significantly larger and full-precision counterparts.
- For a deeper understanding of these patterns, we analyze these compressed models through the lens of Fourier sensitivity analysis. This offers a much needed explanation for the apparent robustness differences among model compression methods.
- Leveraging spectral properties of the test data and different frequency biases of the models at hand, we develop a domain-adaptive ensemble CARD-Deck that outperforms the prior baselines at a fraction of their memory footprint.

2 Is the inability to create CARDS fundamental?

To motivate the scientific question of interest, we propose the following CARD hypothesis which we then test through a comprehensive empirical testing of existing model compression techniques.

CARD Hypothesis. *Given a sufficiently overparameterized neural network, a suitable model compression (i.e., pruning and binarization) scheme can yield a compact network with comparable (or higher) accuracy and robustness than the same network when it is trained without compression.*

2.1 Methodology

For a comprehensive analysis of existing pruning methods, we introduce a framework inspired by those in [40, 45] that accommodates pruning methods from traditional-through-emerging paradigms. Specifically, we define the trained subnetwork created by one pruning-retraining cycle as:

$$W_{\text{sparse}} = F_1(W_{k_1}; \mathcal{D}) \odot F_2(W_i; \mathcal{D}, \mathcal{M}, k_2), \quad (1)$$

where \mathcal{D} denotes the training dataset, W_i denotes the weight vector at the start of training iteration i (during initial training, $i < T$), F_1 represents the function that finds the weight-masking vector \mathcal{M} , F_2 represents the function that retrains the weights after \mathcal{M} is found, k_i is the earliest training iteration that F_i requires information from (e.g., weight-vector or learning-rate values), F_1 and F_2 are each applied at the beginning of iteration k_1 , and \odot is the Hadamard (element-wise) product. Using this, the pruning paradigms and representative techniques from these categories considered in this paper are as follows:

- Traditional: $k_1 = k_2$ and $F_2 \neq I$ (identity function);
 - Fine-Tuning (FT) [16]: $W_{\text{sparse}} = F_1(W_T) \odot F_2(W_T; \mathcal{D}, \mathcal{M}, T)$
 - Gradual Magnitude Pruning (GMP) [52]: $W_{\text{sparse}} = F_1(W_t) \odot F_2(W_t; \mathcal{D}, \mathcal{M}, t), t < T$
- Rewinding-based Lottery Ticket: $k_1 = T$ and $k_2 = r, r < T$;
 - Weight Rewinding (LTH) [10, 11]: $W_{\text{sparse}} = F_1(W_T) \odot F_2(W_r; \mathcal{D}, \mathcal{M}, r)$
 - Learning Rate Rewinding (LRR) [40]: $W_{\text{sparse}} = F_1(W_T) \odot F_2(W_T; \mathcal{D}, \mathcal{M}, r)$
- Initialization-based (Strong) Lottery Ticket: $k_1 = k_2 = 0$ and $F_2 = I$.
 - Edgpopup (EP) [38]: $W_{\text{sparse}} = F_1(W_0, \text{binary}; \mathcal{D}) \odot I(W_0, \text{binary})$
 - Biprop (BP) [7]: $W_{\text{sparse}} = F_1(W_0; \mathcal{D}) \odot I(W_0, \text{binarized})$.

As opposed to traditional and rewinding schemes, strong lottery ticket [38] schemes do not require any weight training before or after pruning—a performant network is found at initialization via F_1 . In other words, learning occurs simply by pruning a randomly initialized neural network. Furthermore,

²A detailed discussion on related work is provided in Appendix A.

by design BP performs binarization of the weights to reduce the memory footprint. We note that the precision of the weights in networks trained using EP maintain the same precision as the randomly initialized weights. Hence, EP can also be used to identify binarized networks by randomly initializing the weights to binary values. To take advantage of additional compression, in our experiments with EP the mask \mathcal{M} is learned from a binary-initialized weight vector $W_{0, \text{binary}}$. As BP performs binarization during pruning, a full-precision weight vector W_0 is used when finding \mathcal{M} . See Appendix A.1 for more discussion of the differences between methods in each class. In all of these methods, we make use of global unstructured pruning which allows for different pruning percentages at each layer of the network. We elected to use the hyperparameters specifically tuned for each approach by the developers of each method. Details of this can be found in Appendix B. For a reliable comparison, we make use of convolutional [10], VGG [42] and ResNet [17] style architectures of varying size and train them on CIFAR-10 training set [26]. In particular, we make use of the small Conv-4/6/8 models [10], VGG-19, and ResNet-18. The robustness of each model is determined by computing the Top-1 accuracy on CIFAR-10-C – with 15 different common corruptions from four categories: noise, blur, weather, and digital corruptions [21]. As a baseline, we train 5 realizations of each model without pruning. For each pruning technique, we train 5 realizations at each sparsity level from the set $\{50\%, 60\%, 80\%, 90\%, 95\%\}$ to cover the spectrum of low to high pruning percentages.

2.2 Our findings

Accuracy-robustness comparison of global pruning methods. In Figure 1, we plot our experimental results for different architectures. For each pruning method, we plot the mean (over all realizations) accuracy and robustness values relative to the mean of the dense baseline realizations with error bars extending to the minimum and maximum realization value at each of the aforementioned sparsity levels. The first row of plots in each figure corresponds to Top-1 accuracy on CIFAR-10 while the second row corresponds to Top-1 accuracy on CIFAR-10-C (both relative to the baseline dense/non-compressed models). The mean baseline accuracy and robustness for each architecture is listed as a reference accuracy in the corresponding plot.

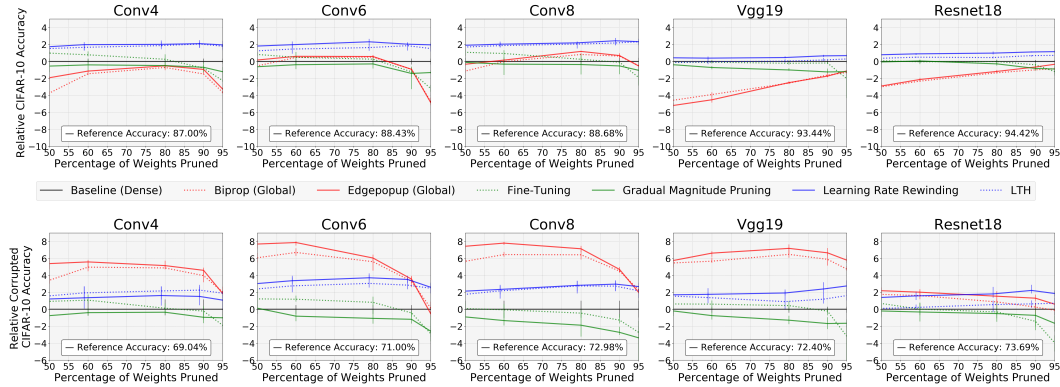


Figure 1: **Suitable pruning approaches dramatically improve robustness over dense models:** Comparing the Top-1 accuracy of pruned models relative to a dense baseline on CIFAR-10 and CIFAR-10-C demonstrates the existence of LRR, LTH, BP and EP CARDS.

Our results for traditional methods, i.e., Fine-Tuning and Gradual Magnitude Pruning, are consistent with previous works [24, 30] as the robustness of models pruned using these methods degrades relative to the dense models’, particularly in higher pruning regimes. However, we find that rewinding and initialization based pruning approaches consistently produce dramatic gains in robustness relative to dense baselines while matching (and sometimes surpassing) the accuracy of the dense baseline. In particular, the rewinding class of methods provide a consistent, moderate improvement to both accuracy and robustness while the initialization class provides more substantial gains in robustness even when the accuracy is slightly below the baseline accuracy. The significance of overparameterization to finding highly compact CARDS using initialization methods is evident for all architecture types, as the robustness of these models in higher pruning regimes improves at increasing levels of parameterization for a given architecture class. However, even in models with fewer parameters, we find that both rewinding and initialization methods are able to provide noticeable robustness gains. Lastly,

the significant robustness gains provided by EP- and BP-pruned models is a feature of initialization pruning methods and not merely due to the weight binarization. We provide a comparison to EP using a full-precision initialization in Appendix C. Another interesting implication of the existence of EP/BP-CARDs is that it shows that within a randomly-initialized neural networks, there exist CARDs which outperform their computationally expensive counterparts without ever modifying the values of the weights.

To summarize, we have empirically verified our hypothesis by demonstrating that “lottery ticket-style” compression methods can identify CARDs. Further, these model compression methods are capable of providing both accuracy and robustness gains over dense models of the same architecture.

Effect of global vs. layerwise pruning in lottery ticket initialization methods. The lottery ticket initialization methods analyzed in the previous section were originally designed to prune a user-specified uniform percentage across all layers of the network. In contrast, global pruning methods are considered to be more flexible as they can prune some layers more heavily than others while still meeting a user-specified sparsity level for the entire network. By analyzing these initialization methods using both layerwise and global pruning, we notice certain peculiar patterns. Figure 2 provides the accuracy and robustness of models trained with BP and EP using global and layerwise pruning. While layerwise-pruned models consistently achieve the maximum accuracy (across prune percentages), the globally-pruned models consistently provide significant robustness gains over the layerwise models. Furthermore, the globally-pruned models typically achieve higher or comparable accuracy at higher sparsity levels, indicating that using initialization methods with global pruning can yield CARDs with better accuracy and robustness at higher level of compactness.

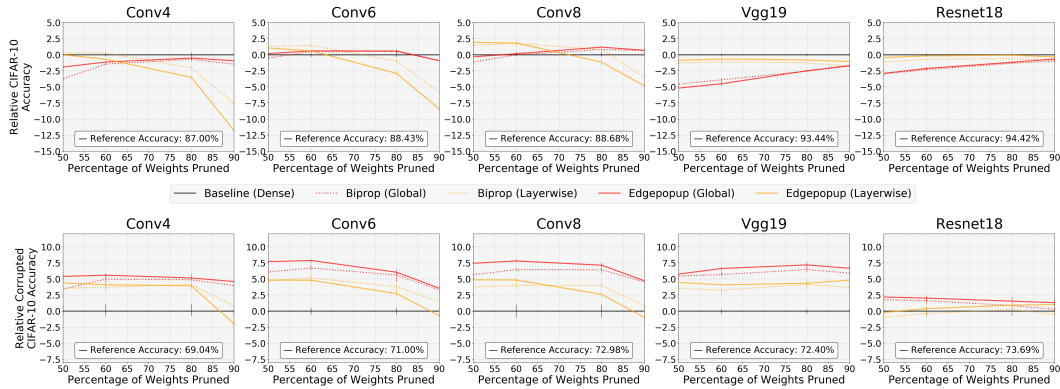


Figure 2: **Global pruning in lottery ticket Initialization methods provides greater robustness gains:** While layerwise pruning is able to achieve the highest accuracy across all sparsity levels in initialization methods, global pruning provides more significant robustness gains at all sparsity levels.

3 A deeper understanding of the effect of compression via a spectral lens

In order to understand what causes these compression methods to have drastically different levels of OoD robustness, we leverage the Fourier sensitivity method [48] to perform a frequency-domain analysis. First, we provide a brief summary of the Fourier sensitivity method. Given a model and a test dataset, we perturb each image in the test dataset with additive Fourier basis noise. Specifically, let X be an image and $U_{i,j} \in \mathbb{R}^{d_1 \times d_2}$ be the 2D Fourier basis matrices. We then compute a perturbed image $X_{i,j} = X + r\epsilon U_{i,j}$, where r is chosen uniformly at random from $\{-1, 1\}$, and $\epsilon > 0$ is the norm of the perturbation. Note that each channel of the image is perturbed independently. After applying this perturbation, we measure the test error for the model under Fourier basis noise and visualize how the test error changes as a function of frequencies (i, j) , thereby yielding the Fourier error heatmap of a model. The heatmap plots the models sensitivity to different frequency perturbations in the Fourier domain. Informally, the center of the heat map contains perturbations corresponding to the lowest-frequency Fourier bases (the clean data) and the edges correspond to the highest frequencies (high frequency noise/corruptions).

We generate error-heatmaps for a trained model corresponding to each pruning method used in Section 2. We also vary the norm of the perturbation, ϵ , over the set $\{3, 4, 6\}$ representing low,

medium, and high levels of perturbation severity. Additionally, we include heatmaps for the dense (non-compressed) baseline model as a reference. Generated heatmaps for the Conv8 architecture at 80% prune percentage are provided in Figure 3; the remaining heatmaps can be found in Section D.

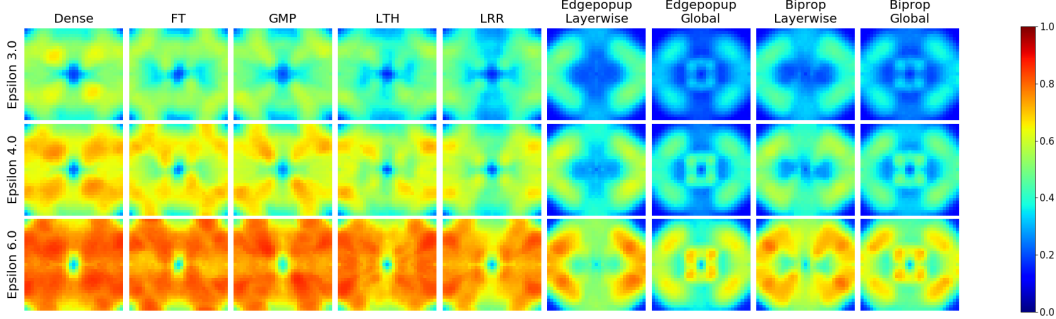


Figure 3: **Visualizing the resilience of compressed models to perturbations at different frequencies:** Fourier heatmaps for error rate of Conv8 trained on CIFAR-10 with 80% pruned weights.

Exploring the cause of robustness differences among different compression methods. Figure 3 illustrates how rewinding and initialization pruning methods reduce the error rate across the whole frequency spectrum of perturbations when compared to the dense rate model. The error rate in initialization-based approaches is lower than the baseline in nearly every heatmap region, aligning with the strong robustness performance of these pruning methods observed in Figure 1. Further, the results for layerwise and global heatmaps indicate that these pruning strategies result in networks that are robust to perturbations of different frequencies. In particular, by comparing the center of the heatmaps for layerwise and global methods, it follows that initialization methods leveraging layerwise pruning are more robust to low frequency perturbations, which translates to a higher accuracy on the clean data. On the other hand, global pruning in initialization methods yields CARs that are less sensitive to mid to high frequency perturbations when compared to layerwise pruned CARs, which translates to a higher robustness to the OoD data. Finally, traditional pruning methods yield a Fourier heatmap with a slightly altered structure when compared to the dense baseline, and it slightly resembles a higher error rate version of heatmaps for rewinding methods. To investigate this, we next provide a more detailed analysis of traditional and rewinding methods.

What separates rewinding methods from traditional pruning methods? While LTH [10] and LRR [40] offer unsurpassed performance, such approaches also greatly extend the training duration, pruning just 20% of the remaining weights every $T - r$ epochs, where T is the initial training duration and r is the epoch the weights/learning-rate are rewound to after each pruning event (here, $r = 12$ and $T = 160$). This raises the question: *Is longer training and the multi-shot pruning procedure critical to the robustness improvements LTH/LRR offer relative to FT/GMP?*

To test this, we gradually construct the LTH/LRR pruning approaches used in this paper by starting from a fine-tuning approach and adding modifications until we produce the LTH/LRR method that prunes the network 13 times to reach 95% sparsity. The phases of this construction for LRR are illustrated in Figure 4, wherein we plot a column of Fourier heatmaps for each phase. Specifically, the first column is our FT approach, the second column extends the fine-tuning duration, the third column adds learning-rate rewinding to this fine-tuning period, the fourth column decreases the iterative prune rate to achieve 95% sparsity in 4 shots rather than 1, and subsequent columns continue to increase the number of pruning shots. In this construction process, we find a notable benefit of adding learning-rate rewinding (70.9% to 72.6% CIFAR-10-C accuracy moving from column 2 to column 3), but the biggest benefits of LTH/LRR come from combining this rewinding with multiple iterations (i.e., all columns from 4 onward display at least 75% robust accuracy). Interestingly, our results also indicate that it may be possible to achieve the robustness benefits of LTH/LRR with a higher iterative pruning rate and thus fewer pruning shots/iterations than what is standard in the literature [10, 40]. Appendix E provides: analogous plots for LTH (at 95% and 90% sparsity) and LRR (at 90% sparsity), which show trends similar to those discussed here, and further discussion.

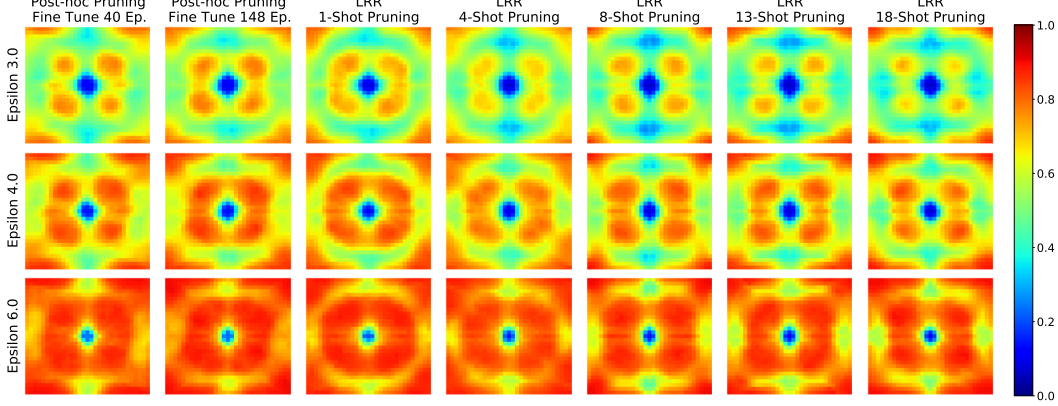


Figure 4: **Comparing the resiliencies of Rewinding and Traditional methods to perturbations at different frequencies:** Fourier heatmaps for error rate of ResNet18 models trained on CIFAR-10 in which 95% of the weights are pruned. From left to right, CIFAR-10-C accuracies: (70.2, 70.9, 72.6, 75.8, 75.2, 75.7, 76.2) and CIFAR-10 accuracies: (93.4, 93.6, 94.5, 95.1, 95.5, 95.7, 95.6).

4 Playing the right CARD to improve accuracy-robustness performance

Our analysis in Section 3 highlights that the robustness of the compressed model on frequency-perturbed data is crucially dependent on the interaction between the frequencies the model is biased towards and the frequencies on which the test-time corruption is concentrated. Motivated by this insight and work on data augmentation methods for biasing the model to improve the robustness, we exploit the compact nature of CARDS to design a test-time ensembling approach based on the spectral similarity of test data and training data.

4.1 Test-time ensembling for improved performance

A spectral-similarity metric. Let $x_{train} \in \mathbb{R}^{D_1 \times D_2 \times N}$ denote the N unaugmented training images of dimension $D_1 \times D_2$, $A = \{a_k\}_{k=1}^m$ denote a set of m different augmentation schemes, and $\hat{S}_{a,P}(x)$ denote a sampling of P images from x where augmentation $a \in A$ has been applied to x . Motivated by our analysis using Fourier heatmaps, we propose a spectral-similarity metric to compare representatives from augmented versions of the training sets, $\{\hat{S}_{a,P}(x_{train})\}_{a \in A}$, to the test data. First, we define $F(\cdot)$ as a map that computes the 1D radially-averaged power spectrum for images of dimension $D_1 \times D_2$ then takes the reciprocal of each component. Our spectral-similarity metric is a map $d_{ss} : \mathbb{R}^{D_1 \times D_2 \times P} \times \mathbb{R}^{D_1 \times D_2 \times M} \rightarrow \mathbb{R}$ defined by $d_{ss}(\mathbf{X}, \mathbf{Y}) = \min_{1 \leq i \leq P} \|(F(X_i)/\|F(X_i)\|) - \frac{1}{M} \sum_{j=1}^M (F(Y_j)/\|F(Y_j)\|)\|$. In practice, we found that the 1D power spectra for different augmentation types were more separable in the higher frequencies of the power spectrum leading to the use of the reciprocal in the definition of $F(\cdot)$. Having proposed this metric, we now leverage it to design a data-adaptive ensembling method.

A “winning hand” of CARDS by test-time ensembling. We now design an ensembling approach called CARD-Deck that leverages the proposed spectral-similarity metric to further improve the performance of CARDS while maintaining a small memory footprint. As a simple baseline, we use a domain-agnostic ensemble that assigns the same weight to all the CARDS in a CARD-Deck. In both ensembling techniques, the ensemble consists of CARDS that have been trained on the same dataset where different augmentation schemes are applied during training. The CARD-Deck ensemble is then composed of n CARDS given by $f^{Deck} = \{f^{a_k}\}_{k=1}^n$ where a_k is one of the m augmentation schemes from A and the superscript in f^{a_k} denotes that this CARD was trained used data from the distribution $S_{a_k}(x_{train})$. When a batch of M test images $x_{test} \in \mathbb{R}^{D_1 \times D_2 \times M}$ is provided to the network, our proposed scheme determines how to leverage the available CARDS in the CARD-Deck to improve the network performance. We provide details on the two variants of CARD-Deck next. A figure illustrating the CARD-Deck design is provided in Appendix F.

Our domain-agnostic CARD-Deck approach makes use of all CARDS in the deck to make the prediction using prediction averaging. Supposing that the output of each CARD in f^{Deck} is softmax vectors, then the output of the static CARD-Deck can be expressed as $\frac{1}{n} \sum_{k=1}^n f^{a_k}(x_{test})$. In our domain-adaptive CARD-Deck, a gating module uses the spectral-similarity metric d_{ss} to determine which augmentation is the most similar to the incoming test images. When an augmentation scheme, say $a \in A$, is identified as the most similar to the incoming test data using d_{ss} , the CARD-Deck selects only the CARDS that were trained using the data from the distribution $\hat{S}_a(x_{train})$. The set of the most similar augmentations is given by $a^* \in \arg \min_{a \in A} d_{ss}(\hat{S}_{a,P}(x_{train}), x_{test})$. We note that a^* is likely to be a singleton set indicating that a single augmentation scheme is most similar. If the CARD-Deck contains multiple cards trained using the same data augmentation scheme, prediction averaging is used on these CARDS and returned as the CARD-Deck prediction. As computing the spectral-similarity scheme is independent of CARD evaluation, the CARD-Deck provides reduced inference time by only evaluating the CARDS necessary for prediction. Given a^* and letting $\mathcal{I}(a) = \{k : a_k \in a\}$, the output of the domain-adaptive CARD-Deck can be expressed as $\frac{1}{|\mathcal{I}(a^*)|} \sum_{k \in \mathcal{I}(a^*)} f^{a_k}(x_{test})$.

4.2 Experimental results

In this section, we compare the performance of CARDS and CARD-Decks with the state-of-the-art techniques. Additional results are provided in Appendix F.

CARDS can leverage state-of-the-art data augmentation techniques. For our experiments, we select two augmentation schemes. The first is AugMix [22] which provides improved robustness without compromising the clean accuracy. The second is a Gaussian noise augmentation where $\mathcal{N}(\mu = 0, \sigma = 0.1)$ is independently added to all the training image pixels with probability $p = 0.5$. We trained CARDS using each pruning and augmentation scheme with the ResNet-18 architecture. The clean and robust accuracies (averaged across three realizations) of CARDS for each pruning scheme are provided in Table 1. We also report the memory usage, calculated using [47]. We find that CARDS perform comparably to (and in some cases better than) their dense counterparts in terms of accuracy and robustness but have a significantly smaller memory footprint.

Test-time ensembling can enable a “winning hand”. We train 3 realizations of CARDS using each pruning and augmentation scheme with the ResNet-18 architecture. For each pruning scheme, we formed CARD-Decks of size 2, 4 and 6, where half of the CARDS are trained using AugMix and the other half are trained using the Gaussian augmentation scheme. When using the spectral-similarity metric in data-adaptive CARD-Decks, we used $P = 5000$ to sample images from $\hat{S}_{AugMix,P}(x_{train})$ and $\hat{S}_{Gaussian,P}(x_{train})$ to use as the representatives for the AugMix and Gaussian datasets in the similarity metric, respectively. At test time, $M = 100$ was the number of test images used in the spectral-similarity metric to determine which augmentation representatives best represented the corrupted test data. Performance of the domain-agnostic and domain-adaptive 2-, 4-, and 6-CARD-Decks with the ResNet-18 architecture are provided in Table 2. We find that both the domain-agnostic and adaptive methods are capable of significantly improving the performance while keeping the memory usage to a minimal level. Specifically, our best performing ResNet-18 CARD-Deck makes use of 6 LRR CARDS (26.87 MB (megabyte) total) and yields clean and robust accuracies of 96.6% and 92.1%, respectively. Furthermore, our EP and BP CARD-Decks achieve clean and robust accuracies in the range of 94.5 – 95.0% and 88.5 – 90%, respectively, while keeping memory usage in the range of 0.15 – 0.42 MB. The memory footprints of our proposed CARD-Decks are dramatically smaller than a single dense ResNet-18 that requires 44.75 MB of parameter memory.

Amplifying performance gains by using larger models. Next, we evaluate whether the performance gains of CARDS can be amplified by using the popular robustness improvement strategy of using larger models. We use the same experimental setting as the previous CARD and CARD-Deck experiments but with larger models – ResNeXt-29, ResNet-50, and WideResNet-18 (2x). While ResNeXt-29 is smaller than ResNet-18, we include it here because like ResNet-50 [4, 6] it is used to establish a well-known benchmark result [22, 6]. Averaged results for ResNeXt-29, ResNet-50 and WideResNet-18 CARDS can be found in Tables 12, 13, and 14 (in Appendix F), respectively. Notably, we found a single LRR CARD (a WideResNet-18 at 96% sparsity) trained with AugMix can attain 91.24% CIFAR-10-C accuracy, outperforming dense ResNeXt-29 trained with AugMix (a state-of-the-art among methods that do not require non-CIFAR-10 training data) by more than

		Baseline			CARD																				
		Dense			Edgepop						LRR						LTH			Biprop					
											Global			Global			Global			Layerwise			Global		
		Augmix	Clean	Gauss.	Augmix	Clean	Gauss.	Augmix	Clean	Gauss.	Augmix	Clean	Gauss.	Augmix	Clean	Gauss.	Augmix	Clean	Gaussian	Augmix	Clean	Gauss.			
80%	Clean Acc.	95.5	95.1	93.9	94.3	93.7	92.4	94.9	94.4	93	96.1	95.6	93.8	95.6	94.9	93.5	93.9	93.7	92.4	94.5	94.1	93.2			
	Robust Acc.	89.2	73.7	85.6	87.8	76.7	85.1	88.4	74.4	85.7	89.8	76.3	86.4	89.4	74.4	85.8	87.5	76.1	85.1	87.8	74.3	85.3			
	Memory (Mbit)	358	358	358	2.23	2.23	2.23	2.23	2.23	2.23	71.5	71.5	71.5	71.5	71.5	71.5	2.23	2.23	2.23	2.23	2.23	2.23			
90%	Clean Acc.	95.5	95.1	93.9	94.4	93.9	92.9	94.9	94.1	92.8	96.3	95.6	93.9	95.7	95.2	93.6	94.4	94.1	92.7	93.7	93.6	93			
	Robust Acc.	89.2	73.7	85.6	88	75.6	85.2	87.9	76	85.4	89.8	75.7	86.3	89.7	76.4	86	87.8	75.1	85	87.1	74.6	84.2			
	Memory (Mbit)	358	358	358	1.12	1.12	1.12	1.12	1.12	1.12	35.8	35.8	35.8	35.8	35.8	35.8	1.12	1.12	1.12	1.12	1.12	1.12			
95%	Clean Acc.	95.5	95.1	93.9	94.5	94	92.6	93.2	92.7	91.2	96.1	95.7	93.9	95.8	95.1	93.8	94.2	93.8	92.5	92.5	92.1	91.4			
	Robust Acc.	89.2	73.7	85.6	87.8	73.1	84.3	85.7	73.4	83.9	89.6	75.6	86.3	89.7	76.5	86	87.5	73.8	84.4	84.7	73.4	83.1			
	Memory (Mbit)	358	358	358	0.56	0.56	0.56	0.56	0.56	0.56	17.9	17.9	17.9	17.9	17.9	17.9	0.56	0.56	0.56	0.56	0.56	0.56			

Table 1: Performance comparison between dense baselines and CARDs using ResNet-18 architecture. Clean and Robust Acc. refer to accuracy on CIFAR-10 and CIFAR-10-C, respectively. The best performance for each method is shown in bold.

		CARD-Deck (Agnostic/Adaptive)											
		Edgepop (Global)			LRR			LTH			Biprop (Global)		
		2	4	6	2	4	6	2	4	6	2	4	6
80%	Clean Acc.	92.1/94.1	94/94.5	94.2/94.8	96/96	96.3/96.4	96.4/96.6	95.5/95.5	96/96.1	96.1/96.1	93.8/93.8	94.3/94.3	94.3/94.4
	Robust Acc.	85/88.9	88.4/89.8	88.9/90	89.7/90.9	91.7/91.8	91.9/92	89.4/90.4	91/91.2	91.2/91.4	87.5/88.6	88.8/89.3	89/89.6
	Memory (Mbit)	4.47	8.94	13.4	143	286	429	143	286	429	4.47	8.94	13.4
90%	Clean Acc.	92.9/94.4	94.6/94.8	94.7/94.8	96.3/96.3	96.4/96.4	96.4/96.6	95.7/95.7	95.9/95.7	96.2/96.2	94/94	94.6/94.4	94.5/94.6
	Robust Acc.	85.2/89.2	88.6/90.1	89.3/90.4	89.8/91.1	91.7/91.8	92/92.1	89.4/90.5	91/91.3	91.3/91.5	87.4/88.6	89.2/89.5	89.4/89.9
	Memory (Mbit)	2.23	4.47	6.70	71.5	143	215	71.5	143	215	2.23	4.47	6.70
95%	Clean Acc.	92.6/94.5	94.2/94.8	94.5/95.1	96.1/96.1	96.3/96.4	96.3/96.5	95.8/95.8	96/96.1	96.1/96.2	94/94	94.7/94.5	94.7/94.6
	Robust Acc.	84.3/88.6	87.7/89.5	88.4/89.9	89.6/91	91.6/91.8	91.9/92	89/90.3	90.8/91.1	91.1/91.4	87.2/88.5	88.9/89.4	89.2/89.7
	Memory (Mbit)	1.12	2.23	3.35	35.8	71.5	107	35.8	71.5	107	1.12	2.23	3.35

Table 2: Performance of domain-agnostic and domain-adaptive ResNet-18 CARD-Decks. Clean and Robust Acc. refer CIFAR-10 and CIFAR-10-C accuracy, respectively.

2% simply by pruning a larger model, i.e., WideResNet-18. In Table 3, we show the results of using the WideResNet-18 architecture for building domain-agnostic and domain-adaptive 2-, 4-, and 6-CARD-Decks. It can be seen that the use of larger models translates to larger gains in performance. Specifically, our best performing 6 LRR CARD-Deck (53.58 MB) sets a new state-of-the-art for CIFAR-10 and CIFAR-10-C accuracies of 96.8% and 92.75%, respectively. In contrast, the previous best method [4] achieves accuracies (94.93%, 92.17%) using a significantly larger model (ResNet-50 with 94.12 MB), extra data (a super resolution network was pre-trained with non-CIFAR-10 data), and a computationally expensive adversarial training procedure. More impressively, our computationally lighter EP and BP CARD-Decks achieve clean and robust accuracies of 95.3% and 90.5%, respectively, while keeping memory usage down to 1.67 MB. Note that the performance of EP and BP CARD-Decks can be further improved by leveraging more computationally expensive training procedures, e.g., searching for EP and BP CARDs in pretrained neural nets.

5 Theoretical justifications

Although our empirical analysis was focused on just one dataset CIFAR-10, here we provide theoretical results that are general and dataset-agnostic.

5.1 Function approximation view of CARDs

By leveraging existing theoretical analyses of the Strong and Multi-Prize Lottery Ticket Hypotheses [37, 36, 7], we next provide theoretical guarantees on the existence and approximation potential of CARDs under certain assumptions. Note that this result does not guarantee the existence of CARDs

		CARD-Deck (Agnostic/Adaptive)											
		Edgepopup (Global)			LRR			LTH			Biprop (Global)		
		2	4	6	2	4	6	2	4	6	2	4	6
90%	Clean Acc.	92.4/ 92.9	94.0/ 94.8	94.8/ 95.1	96.3/ 96.3	96.7/ 96.7	96.7/ 96.8	96.1/ 96.1	96.5/ 96.4	96.6/ 96.6	92.4/ 93.1	94.3/ 94.5	94.9/ 95.0
	Robust Acc.	85.1/ 86.2	88.6/ 90.0	90.1/ 90.6	90.6/ 91.7	92.3/ 92.3	92.5/ 92.6	90.1/ 91.2	91.6/ 91.8	91.9/ 92.1	85.3/ 86.2	88.7/ 89.8	89.9/ 90.5
	Memory (Mbit)	8.93	17.86	26.79	285.8	571.6	857.5	285.8	571.6	857.5	8.93	17.86	26.79
95%	Clean Acc.	92.8/ 93.4	94.6/ 94.9	95.1/ 95.3	96.3/ 96.3	96.8/ 96.8	96.6/ 96.8	96.1/ 96.1	96.5/ 96.4	96.6/ 96.7	92.3/ 92.8	94.2/ 94.5	95.0/ 95.2
	Robust Acc.	85.2/ 86.1	88.6/ 89.9	90.0/ 90.6	90.8/ 91.8	92.4/ 92.5	92.7/ 92.75	89.9/ 91.4	91.6/ 91.9	91.9/ 92.2	84.9/ 86.0	88.4/ 89.5	90.0/ 90.5
	Memory (Mbit)	4.46	8.93	13.39	142.9	285.8	428.7	142.9	285.8	428.7	4.46	8.93	13.39

Table 3: Performance of domain-agnostic and domain-adaptive WideResNet-18 CARD-Decks. Clean and Robust Acc. refer to CIFAR-10 and CIFAR-10-C accuracy, respectively. The best performance for each method is shown in bold. For reference, dense WideResNet-18 (Augmix) model achieves (Clean Acc., Robust Acc., Memory) = (95.6%, 89.3%, 1429 Mbit).

with the same size network as the dense network even though we were able to empirically demonstrate such CARDS exist. We state an informal version of this result for binary-weight CARDS here.

Theorem 1. (*Informal Statement of CARD Approximation Theorem*) *Given a non-compressed network F with depth ℓ and width w with bounded weights that achieves a desired target accuracy and robustness, a random binary network of depth 2ℓ and width $O((\ell w^{3/2}/\varepsilon) + \ell w \log(\ell w/\delta))$ contains with probability $(1-\delta)$ a binary-weighted CARD that approximates the target non-compressed network with error at most ε , for any $\varepsilon, \delta > 0$.*

We note that the CARD Approximation Theorem follows immediately from Theorem 2 in [7]. Hence, for a formal version of Theorem 1 we refer the reader to Theorem 2 in [7]. This result provides a level of confidence with which one can expect to find a binary-weight CARD that is an ε -approximation of a target (i.e. trained and non-compressed) network, in sense of the Euclidean norm. Note that the bound on the width and depth of the randomly initialized network containing a CARD that is an ε -approximation of the non-compressed target network pertains specifically to binary-weight CARDS. For full-precision weight CARDS, tighter bounds on the depth and width of a fully-connected network with ReLU activations containing a CARD that is an ε -approximation of a target network follow from Theorem 3 in [36]. Further, Theorem 3 in [36] establishes that the existence of these full-precision CARDS under a more relaxed hypothesis set than that required to establish the ε -approximation property for binary-weight subnetworks. Regardless, for both full-precision and binary-weight CARDS theoretical results have been established that can be leveraged to ensure the existence of CARDS, with high probability, provided that these CARDS are searched for within a sufficiently overparameterized network. While these results require the CARDS to be searched for within a network larger than the target network, we note that in our empirical results we were able to find both full-precision and binary-weight CARDS within the same size network architecture as the target network. Leveraging these results establishing the existence of CARDS capable of approximating target networks, we provide a corollary on the approximation capabilities CARD-Deck ensembles. To state this result, we borrow the following notation from [36]. We denote by $F(\ell, \mathbf{w})$ a fully-connected neural network with ReLU activations where ℓ denotes the depth of the network and $\mathbf{w} = [w_0, w_1, \dots, w_\ell] \in \mathbb{N}^{\ell+1}$ is a vector where component $i \in \{1, \dots, \ell\}$ denotes the width of layer i in F and w_0 denotes the input dimension of F . We are now ready to state the corollary.

Corollary 2 (CARD-Deck Approximation Theorem). *Let $\varepsilon > 0$, $\delta > 0$, $n \geq 1$, and $\boldsymbol{\lambda} = [\lambda_1, \dots, \lambda_n]$ satisfying $\sum_{k=1}^n \lambda_k = 1$ and $\lambda_k \geq 0$, for all $k \in [n]$, be given. Let $\mathcal{F} = \{F_k(\ell_k, \mathbf{w}_k)\}_{k=1}^n$ be a deck (collection) of non-compressed fully-connected networks with ReLU activations.*

- 1) *If the input space \mathcal{X} and each network in the collection \mathcal{F} satisfies the hypotheses of Theorem 3 in [36], then with probability $(1-\delta)^n$ there exists a deck of n full-precision CARDS denoted $f^{Deck} = \{f_k\}_{k=1}^n$ of depth and width specified by Theorem 3 in [36] such that*

$$\sup_{x \in \mathcal{X}} \left\| \sum_{k=1}^n \lambda_k f_k(x) - \sum_{k=1}^n \lambda_k F_k(\ell, \mathbf{w})(x) \right\| \leq \varepsilon. \quad (2)$$

- 2) *If the input space \mathcal{X} and each network in the collection \mathcal{F} satisfy the hypotheses of Theorem 2 in [7], then with probability $(1-\delta)^n$ there exists a deck of n binary-weight CARDS denoted*

$f^{Deck} = \{f_k\}_{k=1}^n$ of depth and width prescribed in Theorem 2 of [7] such that

$$\sup_{x \in \mathcal{X}} \left\| \sum_{k=1}^n \lambda_i f_k(x) - \sum_{k=1}^n \lambda_i F_k(\ell, \mathbf{w})(x) \right\| \leq \varepsilon. \quad (3)$$

A proof of Corollary 2 is provided in Appendix G. Note that the target non-compressed networks in Corollary 2 could be trained on data sampled from augmented distributions, such as augmented distributions using the Augmix and Gaussian methods, provided that the weights of the resulting networks satisfy the hypothesis required from the existing results in [36, 7]. Additionally, the appropriate choice of λ in Corollary 2 can yield the domain-agnostic or domain-adaptive CARD-Deck. First, fixing all components of λ to $1/n$ in a collection of n CARs yields the prediction averaging used by the domain-agnostic CARD-Deck. In the domain-adaptive case, the value of λ is dependent on the test data. Suppose the CARD-Deck ensemble contains n CARs given by $f^{Deck} = \{f^{a_k}\}_{k=1}^n$ where a_k is one of the m augmentation schemes from the set of augmentations A and the superscript in f^{a_k} denotes that the CARD was trained used data from the distribution $S_{a_k}(x_{train})$. When the spectral similarity gating function selects $a^* \subseteq A$ for the given test data, taking $\lambda_i = 1/|\mathcal{I}(a^*)|$ for $i \in \mathcal{I}(a^*) = \{i : a_i \in a^*\}$ and 0 otherwise yields the domain-adaptive CARD-Deck.

5.2 Robustness analysis of CARD-Deck

To provide the theoretical justification behind our CARD-Deck approach over a single classifier, we first define a robustness measure for a given classifier ensemble trained on a set of augmentations w.r.t. a corruption set encountered at the test-time. We assume that each test sample may encounter a specific corruption type c from a given OoD set and be transformed to a corrupted test sample x_c . Let us assume f^a is learnt using a learning algorithm L using the augmented training data S_a sampled from distribution \mathcal{D}_a , thus, we have $f^{Deck} = \{f^a = L(S_a) | a \in \mathbb{N}^A\}$ where $\mathbb{N}^A = \{1, \dots, A\}$. Let us denote by \hat{S}_a an empirical distribution w.r.t. sampled dataset S_a .

Definition 1 (Average OoD Robustness). *Let $f^{Deck} = \{f^a | a \in \mathbb{N}^A\}$ denote a CARD-Deck trained using an augmentation set $S^A = \{S_a \sim \mathcal{D}_a | a \in \mathbb{N}^A\}$. We define the average out-of-distribution robustness for a CARD-Deck w.r.t. corruption set $\mathcal{D}^C = \{\mathcal{D}_c | c \in \mathbb{N}^C\}$ as*

$$Rob(\mathcal{D}^C, f^{Deck}) = \sum_{a=1}^{|\mathcal{A}|} \sum_{c=1}^{|\mathcal{C}|} Rob(\mathcal{D}_c, f^a) w_c^a, \quad (4)$$

where $Rob(\mathcal{D}_c, f^a) = \mathbb{E}_{(x_c, y) \sim \mathcal{D}_c} [\inf_{f^a(x'_c) \neq y} d(x'_c, x_c)]$ with x'_c being a perturbed version of x_c , d corresponds to a distance metric, and w_c^a denotes the probability of f^{Deck} gating module selecting the classifier f^a to make a prediction on test data coming from corruption type c .

This definition refers to the expectation of the distance to the closest misclassified corrupted sample for a given test sample. Note that this is a stronger notion of robustness than the generalization error corresponding to a corrupted data distribution. Having this definition, our goal is to provide a lower bound on the average OoD robustness of f^{Deck} and show that the use of domain-adaptive classifier ensemble achieves a better OoD robustness compared to the case where we use just a single classifier f^a . To understand this quantity better, we derive the following decomposition (see Appendix G for more details):

$$Rob(\mathcal{D}^C, f^{Deck}) \geq \sum_{a,c} w_c^a \underbrace{[Rob(\hat{S}_a, f^a)]}_{(a)} - \underbrace{\|Rob(\mathcal{D}_a, f^a) - Rob(\hat{S}_a, f^a)\|}_{(b)} - \underbrace{\|Rob(\mathcal{D}_c, f^a) - Rob(\mathcal{D}_a, f^a)\|}_{(c)}.$$

This shows that we can bound the average OoD robustness from below in terms of the following three error terms for a classifier-corruption pair weighted by their gating (or selection) probabilities: (a) empirical robustness, (b) generalization gap, and (c) out-of-distribution-shift.

This inequality suggests that in order to bound the average OoD robustness, we need to bound both the generalization gap and the OoD-shift. Next, we provide a bound on the OoD-shift penalty that is independent of the classifier f^a and is only related to the closeness of the augmented data distribution and corrupted data distribution. Specifically, the closeness is defined in terms of Wasserstein distance $W(\cdot, \cdot)$ as defined in Definition 2 in Appendix G.

Theorem 3 (Average OoD-Shift Bound). *For any CARD-Deck, the average OoD-shift (i.e., $ADS = \sum_{a,c} w_c^a \|Rob(\mathcal{D}_c, f^a) - Rob(\mathcal{D}_a, f^a)\|$) can be bounded as follows*

$$ADS \leq \sum_{a=1}^{|A|} \sum_{c=1}^{|C|} w_c^a \times W(\mathcal{D}_c, \mathcal{D}_a).$$

Proof. This result can be proved by applying Theorem 1 in [41] to ADS. \square

Key insights. Theorem 3 provides some key insights into the OoD robustness of classifiers trained on augmented datasets. First, unlike the generalization gap, the OoD-shift does not converge to zero when more augmentation data is provided from the augmented data distributions. This imposes a fundamental limit on the OoD robustness in terms of the distance between augmented train data distribution and corrupted test data distribution. Second, having diverse augmentations is critical to improving the OoD robustness. Also, it highlights that existing solutions trained with a single augmentation scheme might just be getting lucky or overfitting to the corrupted test data. Finally, the domain-adaptive CARD-Deck with a suitable gating function is provably better than using a single classifier because it can achieve the minimum conditional Wasserstein distance (or best achievable OoD robustness) over given augmentation-corruption pairs.

6 Limitations and future directions

In this paper, we showed that the model compression and high robustness (and accuracy) are not necessarily conflicting objectives. In fact, we found that compression, if done properly (e.g., using “lottery ticket-style” objectives), can dramatically improve the OoD robustness compared to a non-compressed model. Leveraging this finding, we proposed a simple domain-adaptive ensemble of compressed models that outperformed existing SOTA in terms of the clean accuracy and the OoD robustness (at a fraction of the original memory usage).

Our results are consistent with the past results in that we also show that the use of test accuracy alone to evaluate the quality/deployability of a compressed model in the wild is not sufficient—one needs to adopt harder metrics such as OoD robustness. However, as opposed to the existing works in this direction, we present a construction that satisfies these “harder” requirements.

There are still many interesting questions that remain to be explored. First, spectral behavior of train and test data (as considered in this work) is not the only interaction determining the compressed model’s performance. It will be worthwhile to take a more holistic approach that also takes spectral behavior of the compressed model (e.g., using intermediate features) into account when building “a winning hand”. Note that some analytical methodologies used in this paper are certainly exploitable for studying this. Next, our empirical study, though comprehensive in other aspects, was limited to CIFAR-10 dataset. We plan to extend this study to more complex datasets in the near future. Next, we only derived an upper bound on the amount of overparameterization needed to approximate a target dense network in our current theoretical analysis; it will also be interesting to explore a lower bound (a necessary condition) on the same which may indicate scenarios where the proposed approach will not work (e.g., underparameterized NNs). Also, “lottery ticket-style” networks in theory can be found more efficiently, which was not the focus of this work but is a very valuable future direction. Further, achieving the theoretical memory savings obtained from CARDs (reported in this paper) would require their implementation on specialized hardware, e.g., FPGAs. Finally, our technique is compatible with most existing robust training methods and is expected to perform even better if we use bigger models, more advanced and end-to-end robust training with additional augmentation types. This was not considered in the paper as our primary goal was not to push SOTA but to show the existence and some initial constructions of CARDs. We hope that our results, together with our analysis and new algorithmic tools, will help researchers better understand the limits of compressed neural networks and motivate future work in the direction of developing high performing CARDs and CARD-Decks, and their applications to impactful application areas where DL struggles currently due to its parameter-inefficiency and OoD brittleness.

Acknowledgements

This work was performed under the auspices of the U.S. Department of Energy by the Lawrence Livermore National Laboratory under Contract No. DE-AC52-07NA27344, Lawrence Livermore National Security, LLC. This document was prepared as an account of the work sponsored by an agency of the United States Government. Neither the United States Government nor Lawrence Livermore National Security, LLC, nor any of their employees makes any warranty, expressed or implied, or assumes any legal liability or responsibility for the accuracy, completeness, or usefulness of any information, apparatus, product, or process disclosed, or represents that its use would not infringe privately owned rights. Reference herein to any specific commercial product, process, or service by trade name, trademark, manufacturer, or otherwise does not necessarily constitute or imply its endorsement, recommendation, or favoring by the United States Government or Lawrence Livermore National Security, LLC. The views and opinions of the authors expressed herein do not necessarily state or reflect those of the United States Government or Lawrence Livermore National Security, LLC, and shall not be used for advertising or product endorsement purposes. This work was supported by LLNL Laboratory Directed Research and Development project 20-ER-014.

References

- [1] Kshitij Bhardwaj and Maya Gokhale. Semi-supervised on-device neural network adaptation for remote and portable laser-induced breakdown spectroscopy. *arXiv preprint arXiv:2104.03439*, 2021.
- [2] Tom B Brown, Benjamin Mann, Nick Ryder, Melanie Subbiah, Jared Kaplan, Prafulla Dhariwal, Arvind Neelakantan, Pranav Shyam, Girish Sastry, Amanda Askell, et al. Language models are few-shot learners. *arXiv preprint arXiv:2005.14165*, 2020.
- [3] Saikiran Bulusu, Bhavya Kailkhura, Bo Li, Pramod K Varshney, and Dawn Song. Anomalous example detection in deep learning: A survey. *IEEE Access*, 8:132330–132347, 2020.
- [4] Dan A Calian, Florian Stimberg, Olivia Wiles, Sylvestre-Alvise Rebuffi, Andras Gyorgy, Timothy Mann, and Sven Gowal. Defending against image corruptions through adversarial augmentations. *arXiv preprint arXiv:2104.01086*, 2021.
- [5] Matthieu Courbariaux, Yoshua Bengio, and Jean-Pierre David. Binaryconnect: Training deep neural networks with binary weights during propagations. In *Advances in neural information processing systems*, pages 3123–3131, 2015.
- [6] Francesco Croce, Maksym Andriushchenko, Vikash Sehwal, Nicolas Flammarion, Mung Chiang, Prateek Mittal, and Matthias Hein. Robustbench: a standardized adversarial robustness benchmark. *arXiv preprint arXiv:2010.09670*, 2020.
- [7] James Diffenderfer and Bhavya Kailkhura. Multi-prize lottery ticket hypothesis: Finding accurate binary neural networks by pruning a randomly weighted network, 2021.
- [8] Pierre Foret, Ariel Kleiner, Hossein Mobahi, and Behnam Neyshabur. Sharpness-aware minimization for efficiently improving generalization. *arXiv preprint arXiv:2010.01412*, 2020.
- [9] Jonathan Frankle. Openlth: A framework for lottery tickets and beyond, 2020. URL https://github.com/facebookresearch/open_lth.
- [10] Jonathan Frankle and Michael Carbin. The lottery ticket hypothesis: Finding sparse, trainable neural networks. *arXiv preprint arXiv:1803.03635*, 2018.
- [11] Jonathan Frankle, Gintare Karolina Dziugaite, Daniel Roy, and Michael Carbin. Linear mode connectivity and the lottery ticket hypothesis. In *International Conference on Machine Learning*, pages 3259–3269. PMLR, 2020.
- [12] Trevor Gale, Erich Elsen, and Sara Hooker. The state of sparsity in deep neural networks. *arXiv preprint arXiv:1902.09574*, 2019.
- [13] Ian Goodfellow, Yoshua Bengio, Aaron Courville, and Yoshua Bengio. *Deep learning*, volume 1. MIT press Cambridge, 2016.
- [14] Sven Gowal, Chongli Qin, Jonathan Uesato, Timothy Mann, and Pushmeet Kohli. Uncovering the limits of adversarial training against norm-bounded adversarial examples. *arXiv preprint arXiv:2010.03593*, 2020.

- [15] Song Han, Huizi Mao, and William J Dally. Deep compression: Compressing deep neural networks with pruning, trained quantization and huffman coding. *arXiv preprint arXiv:1510.00149*, 2015.
- [16] Song Han, Jeff Pool, John Tran, and William J Dally. Learning both weights and connections for efficient neural networks. *arXiv preprint arXiv:1506.02626*, 2015.
- [17] Kaiming He, Xiangyu Zhang, Shaoqing Ren, and Jian Sun. Deep residual learning for image recognition, 2015.
- [18] Kaiming He, Xiangyu Zhang, Shaoqing Ren, and Jian Sun. Identity mappings in deep residual networks, 2016.
- [19] Yihui He, Xiangyu Zhang, and Jian Sun. Channel pruning for accelerating very deep neural networks. In *Proceedings of the IEEE International Conference on Computer Vision*, pages 1389–1397, 2017.
- [20] Yihui He, Ji Lin, Zhijian Liu, Hanrui Wang, Li-Jia Li, and Song Han. Amc: Automl for model compression and acceleration on mobile devices. In *Proceedings of the European Conference on Computer Vision (ECCV)*, pages 784–800, 2018.
- [21] Dan Hendrycks and Thomas Dietterich. Benchmarking neural network robustness to common corruptions and perturbations. *arXiv preprint arXiv:1903.12261*, 2019.
- [22] Dan Hendrycks, Norman Mu, Ekin D Cubuk, Barret Zoph, Justin Gilmer, and Balaji Lakshminarayanan. Augmix: A simple data processing method to improve robustness and uncertainty. *arXiv preprint arXiv:1912.02781*, 2019.
- [23] Dan Hendrycks, Steven Basart, Norman Mu, Saurav Kadavath, Frank Wang, Evan Dorundo, Rahul Desai, Tyler Zhu, Samyak Parajuli, Mike Guo, et al. The many faces of robustness: A critical analysis of out-of-distribution generalization. *arXiv preprint arXiv:2006.16241*, 2020.
- [24] Sara Hooker, Aaron Courville, Gregory Clark, Yann Dauphin, and Andrea Frome. What do compressed deep neural networks forget? *arXiv preprint arXiv:1911.05248*, 2019.
- [25] Klim Kireev, Maksym Andriushchenko, and Nicolas Flammarion. On the effectiveness of adversarial training against common corruptions. *arXiv preprint arXiv:2103.02325*, 2021.
- [26] Alex Krizhevsky, Geoffrey Hinton, et al. Learning multiple layers of features from tiny images. 2009.
- [27] Alex Krizhevsky, Ilya Sutskever, and Geoffrey E Hinton. Imagenet classification with deep convolutional neural networks. *Advances in neural information processing systems*, 25:1097–1105, 2012.
- [28] Yann LeCun, John S Denker, and Sara A Solla. Optimal brain damage. In *Advances in neural information processing systems*, pages 598–605, 1990.
- [29] Hao Li, Asim Kadav, Igor Durdanovic, Hanan Samet, and Hans Peter Graf. Pruning filters for efficient convnets. *arXiv preprint arXiv:1608.08710*, 2016.
- [30] Lucas Liebenwein, Cenk Baykal, Brandon Carter, David Gifford, and Daniela Rus. Lost in pruning: The effects of pruning neural networks beyond test accuracy. *arXiv preprint arXiv:2103.03014*, 2021.
- [31] Xiaofan Lin, Cong Zhao, and Wei Pan. Towards accurate binary convolutional neural network. In *Advances in Neural Information Processing Systems*, pages 345–353, 2017.
- [32] Zhuang Liu, Mingjie Sun, Tinghui Zhou, Gao Huang, and Trevor Darrell. Rethinking the value of network pruning. *arXiv preprint arXiv:1810.05270*, 2018.
- [33] Christos Louizos, Max Welling, and Diederik P Kingma. Learning sparse neural networks through l_0 regularization. *arXiv preprint arXiv:1712.01312*, 2017.
- [34] Dmitry Molchanov, Arsenii Ashukha, and Dmitry Vetrov. Variational dropout sparsifies deep neural networks. In *International Conference on Machine Learning*, pages 2498–2507. PMLR, 2017.
- [35] Sharan Narang, Erich Elsen, Gregory Diamos, and Shubho Sengupta. Exploring sparsity in recurrent neural networks. *arXiv preprint arXiv:1704.05119*, 2017.
- [36] Laurent Orseau, Marcus Hutter, and Omar Rivasplata. Logarithmic pruning is all you need, 2020.

- [37] Ankit Pensia, Shashank Rajput, Alliot Nagle, Harit Vishwakarma, and Dimitris Papailiopoulos. Optimal lottery tickets via subsetsum: Logarithmic over-parameterization is sufficient, 2021.
- [38] Vivek Ramanujan, Mitchell Wortsman, Aniruddha Kembhavi, Ali Farhadi, and Mohammad Rastegari. What’s hidden in a randomly weighted neural network? In *Proceedings of the IEEE/CVF Conference on Computer Vision and Pattern Recognition*, pages 11893–11902, 2020.
- [39] Mohammad Rastegari, Vicente Ordonez, Joseph Redmon, and Ali Farhadi. Xnor-net: Imagenet classification using binary convolutional neural networks. In *European conference on computer vision*, pages 525–542. Springer, 2016.
- [40] Alex Renda, Jonathan Frankle, and Michael Carbin. Comparing rewinding and fine-tuning in neural network pruning, 2020.
- [41] Vikash Sehwal, Saeed Mahloujifar, Tinashe Handina, Sihui Dai, Chong Xiang, Mung Chiang, and Prateek Mittal. Improving adversarial robustness using proxy distributions. *arXiv preprint arXiv:2104.09425*, 2021.
- [42] Karen Simonyan and Andrew Zisserman. Very deep convolutional networks for large-scale image recognition. *arXiv 1409.1556*, 09 2014.
- [43] Mingxing Tan and Quoc V Le. Efficientnetv2: Smaller models and faster training. *arXiv preprint arXiv:2104.00298*, 2021.
- [44] Bindya Venkatesh, Jayaraman J Thiagarajan, Kowshik Thopalli, and Prasanna Sattigeri. Calibrate and prune: Improving reliability of lottery tickets through prediction calibration. *arXiv preprint arXiv:2002.03875*, 2020.
- [45] Huan Wang, Can Qin, Yulun Zhang, and Yun Fu. Emerging paradigms of neural network pruning. *arXiv preprint arXiv:2103.06460*, 2021.
- [46] Wei Wen, Chunpeng Wu, Yandan Wang, Yiran Chen, and Hai Li. Learning structured sparsity in deep neural networks. *arXiv preprint arXiv:1608.03665*, 2016.
- [47] Yinghao Xu, Xin Dong, Yudian Li, and Hao Su. A main/subsidiary network framework for simplifying binary neural networks. In *Proceedings of the IEEE/CVF Conference on Computer Vision and Pattern Recognition*, pages 7154–7162, 2019.
- [48] Dong Yin, Raphael Gontijo Lopes, Jon Shlens, Ekin Dogus Cubuk, and Justin Gilmer. A fourier perspective on model robustness in computer vision. In *Advances in Neural Information Processing Systems*, volume 32, 2019.
- [49] Chiyuan Zhang, Samy Bengio, Moritz Hardt, Benjamin Recht, and Oriol Vinyals. Understanding deep learning requires rethinking generalization. *arXiv preprint arXiv:1611.03530*, 2016.
- [50] Aojun Zhou, Anbang Yao, Yiwen Guo, Lin Xu, and Yurong Chen. Incremental network quantization: Towards lossless cnns with low-precision weights. *arXiv preprint arXiv:1702.03044*, 2017.
- [51] Shuchang Zhou, Yuxin Wu, Zekun Ni, Xinyu Zhou, He Wen, and Yuheng Zou. Dorefa-net: Training low bitwidth convolutional neural networks with low bitwidth gradients. *arXiv preprint arXiv:1606.06160*, 2016.
- [52] Michael Zhu and Suyog Gupta. To prune, or not to prune: exploring the efficacy of pruning for model compression, 2017.

Supplementary Material: *A Winning Hand*: Compressing Deep Networks Can Improve Out-Of-Distribution Robustness

Here we provide a brief outline of the appendices. In Appendix A, we provide details on relevant past works. In Appendix B, we discuss our experimental setting and relevant hyperparameters. In Appendix C, we show that the gain of EP scheme is not only due to the binarization but also due to the adopted pruning strategy. In Appendix D, we provide Fourier heatmaps for additional pruning rates and architectures. In Appendix E, we provide additional Fourier heatmap results on comparing the rewinding-based schemes with the traditional pruning schemes. In Appendix F, we provide a figure illustrating CARD-Decks as well as additional results for CARD and CARD-Deck experiments. In Appendix G, we provide remaining proof details for our theoretical justification of our CARD-Deck approach. We show the universal approximation power of CARD-Decks and prove that CARD-Deck with a suitable gating function is provably better than using a single classifier.

A Background

A.1 Accuracy preserving model compression

Two popular approaches for model compression are: pruning and quantization.

Pruning. Neural network pruning removes weights [28] or larger structures like filters [29] from neural networks to reduce their computational burden [16, 19] and potentially improve their generalization [46, 33]. As the performance of DNNs has continued to improve with increasing levels of overparameterization [49], production DNNs have grown larger [27, 2], and the need to broadly deploy such models has amplified the importance of compression methods like pruning [16, 15].

In modern networks, pruning the smallest magnitude weights after training then fine-tuning (FT) to recover accuracy lost from the pruning event is surprisingly effective; when the pruning is done iteratively rather than all at once, this approach enables a 9x compression ratio without loss of accuracy [16]. Gradual magnitude pruning (GMP) performs such iterative pruning throughout training rather than after training [35, 52], recovering accuracy lost from pruning events as training proceeds, and matches or exceeds the performance of more complex methods [12].

Another form of magnitude pruning stems from work on the lottery ticket hypothesis (LTH), which posits that the final, sparse subnetwork discovered by training then pruning can be rewound to its state at initialization [10] or early in training [11], then trained in isolation to be comparably accurate to the trained dense network. The associated pruning approach that iteratively trains the network, rewinds the weights (and learning rate schedule) to their values early in training, then trains the subnetwork is referred to here as LTH. A simpler version of this algorithm, learning rate rewinding (LRR) [40], only rewinds the learning rate schedule (not the weights) and achieves a state-of-the-art accuracy-efficiency frontier while being less complex than other competitive approaches [52, 34, 10, 20]. LRR has been shown to offer small improvements to accuracy with not-too-high compression ratio [40]. The authors in [44] proposed calibration mechanisms to find more effective lottery tickets.

Building on the lottery ticket hypothesis, the edge-popup (EP) algorithm introduced a way to find sparse subnetworks at initialization that achieve good performance without any further training [38].

Binarization. Typical post-training schemes have not been successful in binarizing pretrained models with or without retraining to achieve reasonable accuracy. Most existing post-training works [15, 50] are limited to ternary weight quantization. To overcome this limitation, there have been several efforts to improve the performance of binary neural network (BNN) training. This is challenging due to the discontinuities introduced by the binarization, which makes back-propagation difficult. Binaryconnect [5] first showed how to train networks with binary weights within the familiar back-propagation paradigm. Unfortunately, this early scheme resulted in a significant drop in accuracy compared to its full precision counterparts. To improve performance, XNOR-Net [39] proposed adding a real-valued channel-wise scaling factor to improve capacity. Dorefa-Net [51] extended XNOR-Net to accelerate the training process via quantized gradients. ABC-Net [31] improved performance by using more weight bases and activation bases at the cost of increased memory.

Notably, one can exploit the complementary nature of pruning and binarization to combine their strengths. For example, Diffenderfer and Kailkhura [7] produced an algorithm for finding multi-prize lottery tickets (MPTs): sparse, binary subnetworks present at initialization that don't require training.

A.2 Accuracy preserving robust training

While DNN models show impressive generalization in I.I.D. data scenarios [43, 8], the robustness of such models on OoD data (e.g., common corruptions – blurring from camera movement, or noise from low-lighting conditions) is critical to the successful deployment of DL in the wild. To evaluate performance in the presence of such common corruptions, Hendrycks and Dietterich [21] introduced the CIFAR-10-C dataset, which comprises validation images from CIFAR-10 [26] that were exposed to 15 diverse corruption types applied at 5 severity levels.

To achieve high OoD robustness and accuracy, AugMix [22] creates data augmentations at training time by composing randomly-selected augmentation operations from a diverse set, which notably excludes augmentations overlapping with those used to create CIFAR-10-C. Additionally, AugMix utilizes a Jensen-Shannon Divergence consistency loss term to match the predictions between different augmentations of a given image. This approach is expanded on by DeepAugment [23], which inputs clean images to a pretrained image-to-image model, corrupts this model's weights and activations with various operations that distort the typical forward pass, then uses the output images as augmented data. AdversarialAugment (AdA) builds on DeepAugment by generating the weight perturbations performed on the image-to-image models via adversarial training [4]. Also, when used with an appropriately selected perturbation radius and distance metric, adversarial training can serve as a strong baseline against common corruptions [14, 25].

Notably, the state-of-the-art in OoD robustness has historically evolved by leveraging more advanced data augmentation schemes and larger models than prior works [6].

A.3 Methods to design compact-accurate-robust models

Despite its critical need, efforts towards achieving model compactness, high accuracy, and OoD robustness simultaneously have mostly been unsuccessful, to the best of our knowledge.

Hooker et al. [24] analyzed traditional compression techniques and showed that pruned and quantized models have comparable accuracy to the original dense network *but* are far more brittle than non-compressed models in response to small distributional changes that humans are robust to. It is well known that even non-compressed models are very brittle to the OoD shifts. The authors in [24] showed that this brittleness is amplified at higher levels of compression.

Liebenwein et al. [30] corroborated that a pruned model can have similar predictive power to the original one when it comes to test accuracy, while being more brittle when faced with out of distribution data points. They further showed that this phenomenon holds even when considering robust training objectives (e.g., data augmentation). Their results suggest that robustness advances discussed in Sec. A.2 may be suboptimal with model compression approaches unless OoD shifts are known at train time.

Notably, the aforementioned papers only analyze a limited class of pruning methods. Our findings are consistent with [24, 30] on the traditional pruning approaches considered in their respective papers.

B Experiment settings

All codes were written in Python using Pytorch and were run on IBM Power9 CPU with 256 GB of RAM and one to two NVIDIA V100 GPUs. Publicly available code was used as the base for each pruning method for models pruned with FT and GMP³, LTH and LRR⁴, EP⁵ and BP⁶. We added functionality for global pruning in FT, GMP, EP and BP as it is not implemented in existing repositories.

³<https://github.com/RAIVNLab/STR>

⁴https://github.com/facebookresearch/open_lth

⁵<https://github.com/allenai/hidden-networks>

⁶<https://github.com/chrundlle/biprop>

	Learning Rate			LR Schedule		Optimizer		Weight Decay		Epochs		Pruning Details	
	Conv2	Conv4/6/8	Rest	Conv2/4/6/8	Rest	Conv2/4/6/8	Rest	Conv2/4/6/8	Rest	Conv2/4/6/8	Rest	Conv2/4/6/8	Rest
Dense	2e-4	3e-4	0.1	None	LR160	Adam	SGD	0	1e-4	100	160	N/A	N/A
FT	← 0.01 →	← 0.1 →	0.1	Cosine	LR160	← SGD →	← SGD →	← 1e-4 →	← 1e-4 →	← 200 →	← 200 →	← Prune at epoch 160 then fine tune 40 epochs →	
GMP	← 0.01 →	← 0.1 →	0.1	Cosine	LR160	← SGD →	← SGD →	← 1e-4 →	← 1e-4 →	← 160 →	← 160 →	← $(s_i, t, n, \Delta t) = (0, 5, 105, 1)$ →	
LTH	5e-3	1e-2	0.1	← LR160 →	← LR160 →	← SGD →	← SGD →	← 1e-4 →	← 1e-4 →	← 160 →	← 160 →	rewind it.: 1000, rate: 20% rewind it.: 5000, rate: 20%	
LRR	5e-3	1e-2	0.1	← LR160 →	← LR160 →	← SGD →	← SGD →	← 1e-4 →	← 1e-4 →	← 160 →	← 160 →	rewind it.: 1000, rate: 20% rewind it.: 5000, rate: 20%	
BP	← 0.1 →	← 0.1 →	← 0.1 →	← Cosine →	← Cosine →	← SGD →	← SGD →	← 1e-4 →	← 1e-4 →	← 250 →	← 250 →	← All Epochs →	
EP	← 0.1 →	← 0.1 →	← 0.1 →	← Cosine →	← Cosine →	← SGD →	← SGD →	← 1e-4 →	← 1e-4 →	← 250 →	← 250 →	← All Epochs →	

Table 4: Hyperparameters used when training dense baselines and each pruning method by model. Note that “Rest” refers to all other models trained in our experiments, such as VGG and ResNet.

Rewinding strategies, LRR and LTH, make use of regular ResNet-18 models while all other methods, including dense, make use of PreAct ResNet-18 [18] as it provided improved performance in terms of accuracy and robustness. We use the following datasets: CIFAR-10 and CIFAR-10-C.

A breakdown of hyperparameters by model and pruning method is provided in Table 4. As mentioned in Section 2, for each pruning method we used hyperparameters tuned specifically for that method. The dense Conv2/4/6/8 models used a batch size of 60, as specified in Figure 2 of the original Lottery Ticket Hypothesis paper [10]. All pruned models and the remaining dense models were trained using a batch size of 128. In the LR schedule column, *Cosine* denotes cosine decay while *LR160* denotes a schedule that sets the learning rate to 0.01 at epoch 80 and 0.001 at epoch 120. All models trained using SGD use a momentum of 0.9.

We first note details of experiments using traditional pruning methods, fine-tuning (FT) and gradual magnitude pruning (GMP). For FT models, unpruned training takes place for 160 epochs at which point pruning to the full sparsity level takes place using global magnitude pruning. After pruning, fine-tuning of the pruned network takes place over 40 epochs where the learning rate is kept at the final value after pruning at epoch 160 [32, 40]. For GMP models, the sparsity level gradually increases over the course of the training process. In our experiments, the sparsity level at training step t increases in accordance with equation (1) from [52] which we include here to interpret the GMP pruning details from Table 4:

$$s_t = s_f + (s_i - s_f) \left(1 - \frac{t - t_0}{n\Delta t}\right)^3, \text{ for } t \in \{t_0 + k\Delta t\}_{k=0}^n. \quad (5)$$

Here, s_i denotes the initial sparsity level, s_f denotes the final sparsity level, n denotes the number of pruning steps, t_0 denotes the first training step where pruning is performed, and s_t denotes the sparsity level at the current training step. Note that the values for s_i , t_0 , n , and Δt are provided in Table 4.

For rewinding methods, LTH and LRR, hyperparameters were chosen based on details from [10, 11, 9, 40]. Notably, our rewinding-iteration choices stemmed from the hyperparameter study shown in Figure 7 of [11], and the fact that the small Conv models performed well when rewound to iteration 0 in [10]. All LTH/LRR runs were implemented using a modified version of the OpenLTH repository [9].

For initialization methods, edgpopup (EP) and biprop (BP), pruning is achieved by learning a pruning mask that is applied to the randomly initialized networks weights and, in the case of BP, binarization is applied to the weights of the resulting pruned network. For EP networks, weights were initialized using the signed constant initialization from [38] which offered the best performance. As an added benefit for compactness, this initialization also yields a binary weight network. For BP networks, weights were initialized using the kaiming normal initialization as in [7]. Due to the binary weights in both the EP and BP CARDS we trained, these CARDS provided further reductions in on-device memory consumption over rewinding based pruning strategies. For both EP and BP, we used the same number of epochs for training as in [7].

C Comparison of full-precision-weight Edgpopup pruning with binary-weight Edgpopup pruning

The models pruned using EP in our experiments are pruned using weights initialized from a scaled binary initialization, as specified in [38]. Additionally, models pruned with BP contain binary weights regardless of the initialization used. To demonstrate that the robustness gains afforded are a feature of initialization based pruning methods and not binarization, we provide some results for full-precision initialization based pruning models. In particular, by using the kaiming normal initialization with EP the resulting network has full-precision weights. In Figure 5, we visualize the accuracy of these models on CIFAR-10 and CIFAR-10-C. While the gains in robustness of these full-precision weight CARDs are not as significant as the binary weight CARDs, these experiments demonstrate the robustness of the initialization based CARDs is not exclusive to binary weight networks.

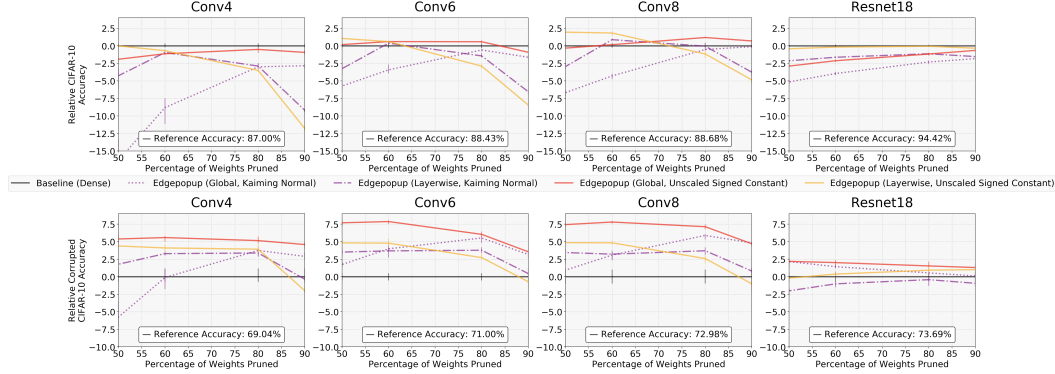


Figure 5: **Using Full Precision weights in lottery ticket Initialization still provides robustness gains:** While initialization pruning methods with binary weights yield the greatest robustness gains over the baseline, randomly initialized networks with full-precision weights pruned using Edgpopup still provide improved robustness over the dense baseline.

D Additional heatmaps

Here we provide additional heatmaps (varying sparsity levels) for Conv8 (see Figures 6 and 7) and for ResNet18 models (see Figures 8, 9 and 10). By comparing the heatmaps of rewinding and initialization based pruning methods to baselines, we find that these models are more resilient to perturbations of varying severity.

D.1 Additional Conv8 heatmaps

In the Conv8 models, significant differences in the heatmaps of initialization methods and the baseline model persist up to the highest sparsity level of 95%, as seen in Figure 7.

D.2 ResNet-18 heatmaps

Here we provide Fourier error rate heatmaps for the ResNet-18 architecture trained using different pruning methods. As in the Conv8 heatmap figures, we include heatmaps for a trained dense ResNet-18 model for reference.

E Constructing iterative pruning with rewinding from fine-tuning

In Section 3, we visualized the Fourier heatmaps for the first replicate of several pruning methods: fine-tuning (40 epochs), fine-tuning with a lengthened fine-tuning duration (148 epochs), fine-tuning with a lengthened fine-tuning duration and learning rate rewinding (i.e., 1-shot LRR pruning), and LRR pruning with 4, 8, 13, and 18 shots. The accuracies listed in the Figure 4 caption are averages of the two (three, for FT methods) replicates we ran for each method. Here, we repeat this experiment

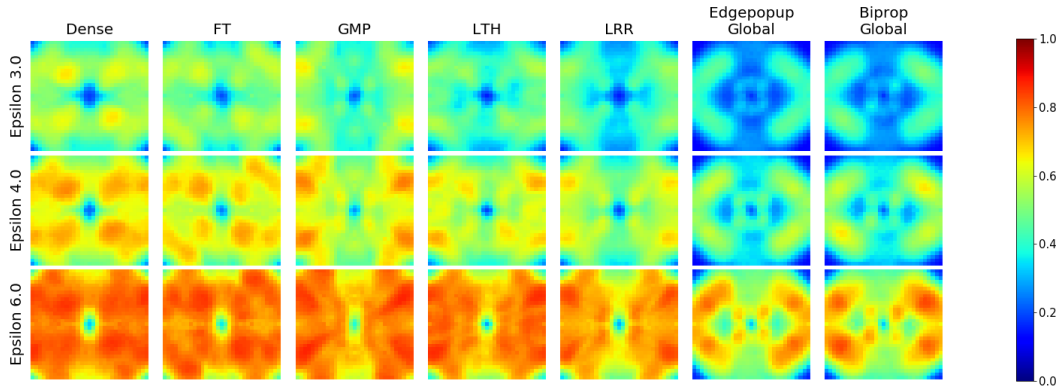


Figure 6: **Visualizing the resilience of compressed models to perturbations at different frequencies:** Fourier heatmaps for error rate of Conv8 trained on CIFAR-10 with 90% pruned weights.

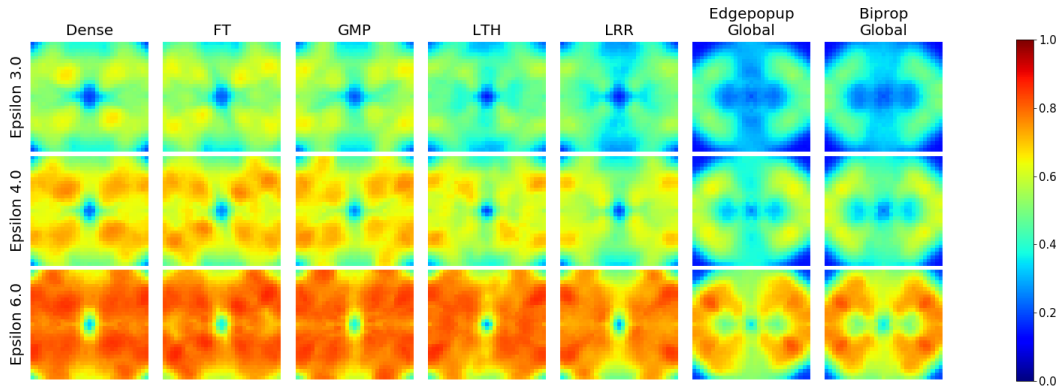


Figure 7: **Visualizing the resilience of compressed models to perturbations at different frequencies:** Fourier heatmaps for error rate of Conv8 trained on CIFAR-10 with 95% pruned weights.

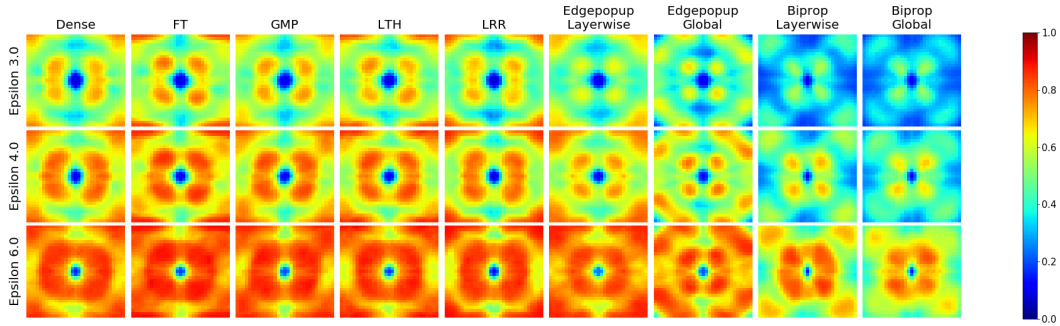


Figure 8: **Visualizing the resilience of compressed models to perturbations at different frequencies:** Fourier heatmaps for error rate of ResNet-18 trained on CIFAR-10 with 80% pruned weights.

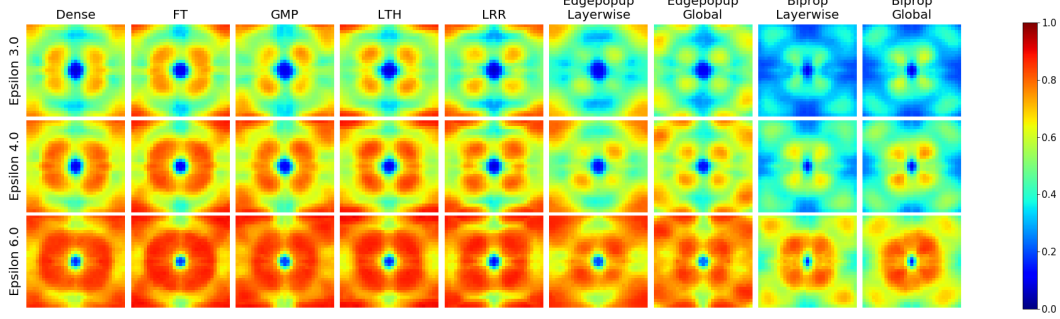


Figure 9: **Visualizing the resilience of compressed models to perturbations at different frequencies:** Fourier heatmaps for error rate of ResNet-18 trained on CIFAR-10 with 90% pruned weights.

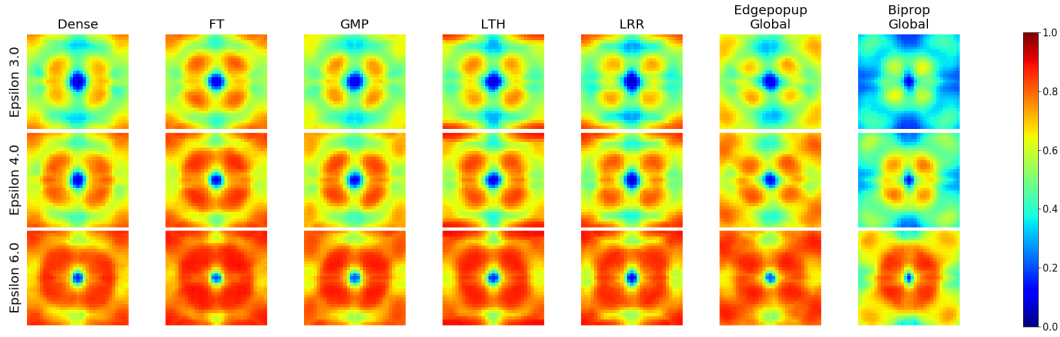


Figure 10: **Visualizing the resilience of compressed models to perturbations at different frequencies:** Fourier heatmaps for error rate of ResNet-18 trained on CIFAR-10 with 95% pruned weights.

using 90% sparsity (Figure 12), using LTH instead of LRR at 95% sparsity (Figure 11), and using LTH and 90% sparsity (Figure 13).

At 95% sparsity, we observe the same pattern we saw in the main text: adding multiple shots of pruning is critical to improving the LTH heatmaps and robustnesses of the rewinding-based methods (Figure 11). That is to say, adding rewinding and a longer post-pruning fine-tuning duration to our FT method is not sufficient to obtain the results achievable with LTH/LRR—multiple iterations are needed. Interestingly, as especially visible at epsilon 6.0 in the Fourier heatmaps, LRR (Figure 4) is clearly more resilient to perturbations than LTH, which is consistent with the improved performance of LRR relative to LTH.

At 90% sparsity, for both LTH (Figure 13) and LRR (Figure 12), the Fourier heatmaps reflect benefits of multiple shots and rewinding (particularly near the centers of the images for all epsilons). For LRR, there is greater similarity among the Rewinding and Initialization Fourier heatmaps at 90% sparsity than at 95% sparsity, and this is reflected in their robustnesses in the captions, which are less separated in the 90% sparsity case. Notably, however, all these robustness figures are consistent with the aforementioned heatmap improvements in that they show the benefits of combining rewinding with multiple pruning shots. Note that 10-shot pruning corresponds to the scheme / iterative pruning rate (20%) we use to reach 90% sparsity in other sections (e.g., Figure 9).

F Additional results with CARDS and CARD-Deck

In this section, we first present an illustrative diagram of the proposed domain-adaptive CARD-Deck scheme in Figure 14.

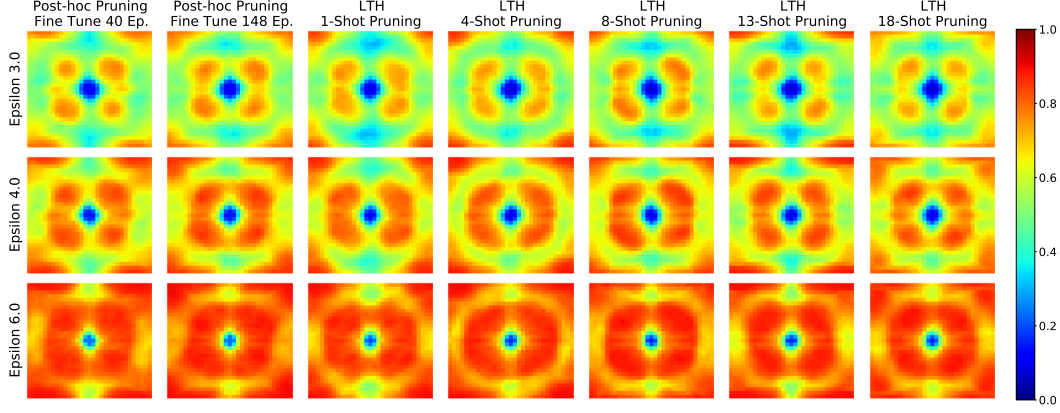


Figure 11: **Comparing the resiliencies of Rewinding and Traditional methods to perturbations at different frequencies:** Fourier heatmaps for error rate of ResNet18 models trained on CIFAR-10 in which 95% of the weights are pruned via LTH. From left to right, CIFAR-10-C accuracies: (70.2, 70.9, 72.1, 74.3, 74.2, 73.9, 74.4) and CIFAR-10 accuracies: (93.4, 93.6, 94.4, 95.0, 95.2, 95.1, 95.2).

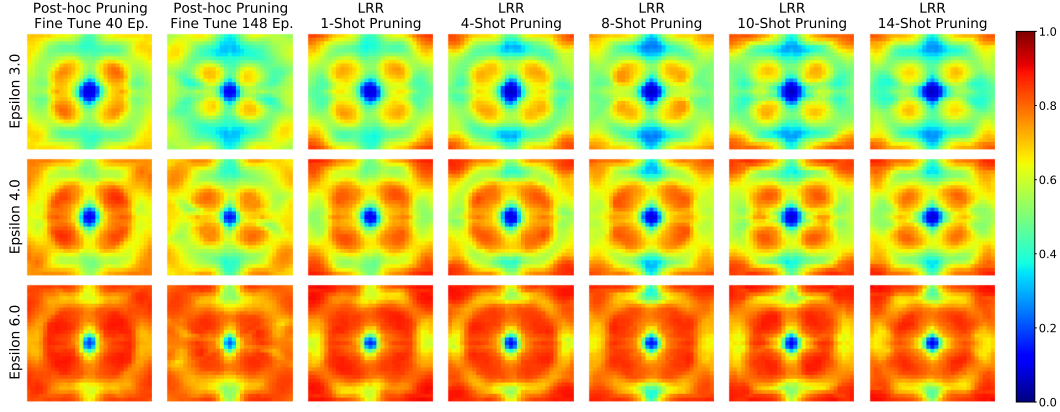


Figure 12: **Comparing the resiliencies of Rewinding and Traditional methods to perturbations at different frequencies:** Fourier heatmaps for error rate of ResNet18 models trained on CIFAR-10 in which 90% of the weights are pruned via LRR. From left to right, CIFAR-10-C accuracies: (72.6, 73.2, 73.8, 75.3, 75.6, 76.1, 76.2) and CIFAR-10 accuracies: (94.2, 94.2, 94.9, 95.4, 95.4, 95.6, 95.5).

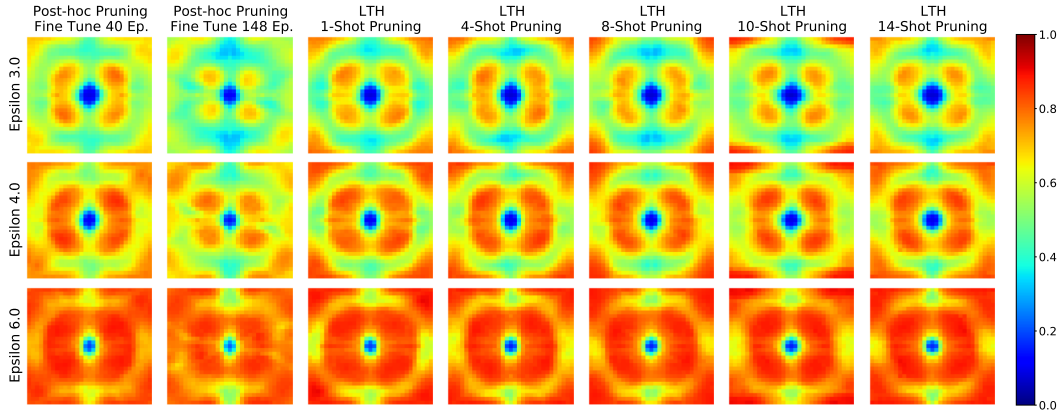


Figure 13: **Comparing the resiliencies of Rewinding and Traditional methods to perturbations at different frequencies:** Fourier heatmaps for error rate of ResNet18 models trained on CIFAR-10 in which 90% of the weights are pruned via LTH. From left to right, CIFAR-10-C accuracies: (72.6, 73.2, 74.1, 74.9, 74.3, 74.5, 74.8) and CIFAR-10 accuracies: (94.2, 94.2, 94.7, 95.0, 95.1, 95.1, 95.1).

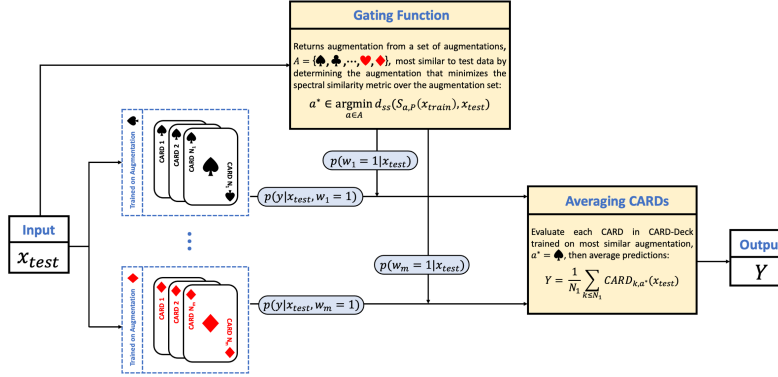


Figure 14: **Selecting a Winning Hand using a Domain-Adaptive CARD-Deck Ensemble:** CARDs are grouped based on the augmentation scheme applied to the data during training. When test data is provided to the CARD-Deck, a gating function attempts to identify the augmentation scheme with data most similar to the incoming test data. The CARDs trained using this data augmentation scheme are evaluated on the test data and the average of their predictions is returned as the CARD-Deck output.

F.1 Additional results for CARDs and CARD-Decks with ResNet-18

In this section, we provide a breakdown of the accuracy of ResNet-18 CARDs and CARD-Decks by CIFAR-10-C corruption types. In particular, Tables 5 - 7 contain the performance of CARDs trained on clean, Augmix, and Gaussian augmentations when tested on CIFAR-10-C corruption types. Tables 8 to 10 contain the performance of LTH, LRR, EP, and BP CARD-Decks on individual CIFAR-10-C corruptions.

As a note of interest, we found that the best performance on different CIFAR-10-C corruptions changes for individual CARDs as the sparsity level increases. At 80% sparsity, a Gaussian CARD yields the highest accuracy on impulse noise but at 90% and 95% sparsity levels Augmix CARDs deliver the highest accuracy on impulse noise. Further, at 95% sparsity the margin of difference in accuracy on impulse noise provided by the Augmix CARD over the Gaussian CARD is more significant.

While pruning using FT and GMP were unable to yield CARDs, note that we include the accuracy and robustness of ResNet-18 models pruned using FT and GMP with the same augmentation schemes in Table 11 for comparison against the performance of ResNet-18 CARDs in Table 1.

F.2 Achieving state-of-the-art performance on CIFAR-10-C using larger models

We report these results in Tables 12, 13 and 14. To summarize, our results highlight the fact that the accuracy/robustness gains due to the model compression (and ensembling) are compatible with the gains from the existing strategies, i.e., data augmentation and the use of larger models. By combining these strategies with the scheme proposed in this paper, we achieve even larger gains in terms of robustness and accuracy, in turn, establishing a new SOTA. Note that we include performance of WideResNet-18 CARD-Decks composed of layerwise pruned BP and EP models in Table 15.

F.3 Note on gating function performance

In Table 16, we provide a break down of the performance of the spectral-similarity based gating function by CIFAR-10-C corruption type. For each augmentation scheme and corruption type, the corresponding number indicates the percentage of data from that corruption selected by the gating function averaged across the 5 severity levels in CIFAR-10-C. Based on the performance of Augmix and Gaussian CARDs by CIFAR-10-C corruption type in Tables 5 - 7, entries in the table are marked in bold whenever a model pruned to sparsity 80%, 90%, or 95% trained using that data augmentation scheme achieved the highest accuracy averaged over all severity levels of that corruption type. Bolding these entries in Table 16 indicates that the gating function typically selects the best performing augmentation scheme, and thereby the CARDs in the deck trained on data most similar to the incoming test data, for the domain-adaptive CARD-Decks. Improvements could be

made by determining a gating function that is more accurate on the frost and jpeg corruptions. As noted in Section F.1, the augmentation scheme yielding the best performing models on impulse and glass corruptions varies with the sparsity level of the pruned network. This observation indicates that an alternative similarity metric that takes into account features of the trained CARDS, such as sparsity level, could provide a gating function that offers improved performance on CIFAR-10-C corruptions.

G Theory

G.1 Proof of Corollary 2

For the sake of clarity, we prove the result 1) but note that the same argument can be applied to yield result 2) by leveraging the hypotheses of Theorem 2 in [7]. Using the triangle inequality, we have that

$$\left\| \sum_{k=1}^n \lambda_i f_k(x) - \sum_{k=1}^n \lambda_i F_k(\ell, \mathbf{w})(x) \right\| \leq \sum_{k=1}^n \lambda_i \|f_k(x) - F_k(\ell, \mathbf{w})(x)\|, \quad (6)$$

for any $x \in \mathcal{X}$. Hence, if

$$\sup_{x \in \mathcal{X}} \|f_k(x) - F_k(\ell, \mathbf{w})(x)\| \leq \varepsilon \quad (7)$$

for each $1 \leq k \leq n$, then it immediately follows that

$$(\ell, \mathbf{w}) \left\| \sum_{k=1}^n \lambda_i f_k(x) - \sum_{k=1}^n \lambda_i F_k(\ell, \mathbf{w})(x) \right\| \leq \sum_{k=1}^n \lambda_i \varepsilon = \varepsilon, \quad (8)$$

for all $x \in \mathcal{X}$. Under the hypotheses of Theorem 3 in [36], for each $k \in \{1, \dots, n\}$ we have that with probability $(1 - \delta)$ there exists a full-precision CARD satisfying (7). Thus, with probability $(1 - \delta)^n$ there exists a collection of full-precision networks $\{f_k\}$ satisfying (2).

G.2 OoD Robustness analysis

To understand the average OoD robustness better, we derive the following decomposition:

$$\begin{aligned} \text{Rob}(\mathcal{D}_c, f^a) &= \text{Rob}(\hat{S}_a, f^a) \\ &+ [\text{Rob}(\mathcal{D}_a, f^a) - \text{Rob}(\hat{S}_a, f^a)] \\ &+ [\text{Rob}(\mathcal{D}_c, f^a) - \text{Rob}(\mathcal{D}_a, f^a)]. \end{aligned}$$

Next, using the triangle inequality $a + (b - a) \geq a - \|b - a\|$ which is true because $\|b - a\| \geq a - b$ for $a, b \geq 0$, we have

$$\begin{aligned} \text{Rob}(\mathcal{D}_c, f^a) &\geq \text{Rob}(\hat{S}_a, f^a) \\ &- \|\text{Rob}(\mathcal{D}_a, f^a) - \text{Rob}(\hat{S}_a, f^a)\| \\ &- \|\text{Rob}(\mathcal{D}_c, f^a) - \text{Rob}(\mathcal{D}_a, f^a)\|. \end{aligned}$$

By linearity of expectation, we can bound (4) from below

$$\text{Rob}(\mathcal{D}^C, f^{\text{Deck}}) \geq \sum_{a=1}^{|A|} \sum_{c=1}^{|C|} w_c^a \text{Rob}(\hat{S}_a, f^a) \quad (9)$$

$$- \sum_{a=1}^{|A|} \sum_{c=1}^{|C|} w_c^a \|\text{Rob}(\mathcal{D}_a, f^a) - \text{Rob}(\hat{S}_a, f^a)\| \quad (10)$$

$$- \sum_{a=1}^{|A|} \sum_{c=1}^{|C|} w_c^a \|\text{Rob}(\mathcal{D}_c, f^a) - \text{Rob}(\mathcal{D}_a, f^a)\|. \quad (11)$$

Note that we have bounded (4) in terms of the following three error terms for a classifier-corruption pair weighted by their gating (or selection) probabilities: 1) empirical robustness (9), 2) generalization gap (10), and 3) OoD-shift (11).

Next, we aim to provide a bound on the OoD-shift that is independent of the classifiers in hand and is only related to the properties of the distributions. To facilitate this, we define a notion of distance between two distributions.

Definition 2 (Conditional Wasserstein distance). *For two labeled distributions \mathcal{D} and \mathcal{D}' with supports on $X \times Y$, we define conditional Wasserstein distance according to a distance metric d as follows:*

$$W(\mathcal{D}, \mathcal{D}') = \mathbb{E}_{(\cdot, y) \sim \mathcal{D}} \left[\inf_{J \in \mathcal{J}(\mathcal{D}|y, \mathcal{D}'|y)} \mathbb{E}_{(x, x') \sim J} d(x, x') \right], \quad (12)$$

where $\mathcal{J}(\mathcal{D}, \mathcal{D}')$ is the set of joint distributions whose marginals are identical to \mathcal{D} and \mathcal{D}' .

Conditional Wasserstein distance between the two distributions is simply the expectation of Wasserstein distance between conditional distributions for each class.

Model	Noise			Blur			Weather			Digital									
	Clean	Avg. Robust	Memory (Mbit)	gaussian	shot	impulse	defocus	glass	motion	zoom	snow	frost	fog	brightness	contrast	elastic	pixelate	jpeg	
Baseline	Dense (Augmix)	95.5	89.2	358	81.7	85.9	86.7	94.3	80.8	92.4	93.2	90.0	89.7	92.2	94.7	91.0	90.5	88.7	87.7
	Dense (Gaussian)	93.9	85.6	358	91.3	91.8	88.3	85.8	81.0	80.9	84.9	86.4	88.3	81.9	92.3	70.6	86.6	88.1	89.9
	Dense (Clean)	95.1	73.7	358	46.5	59.1	54.0	81.8	55.1	78.1	76.4	82.4	78.2	88.2	93.5	78.2	84.0	76.1	79.3
CARDs	LRR (Augmix)	96.1	89.8	71.5	78.5	85.0	88.6	95.1	81.3	93.6	94.2	91.4	90.8	93.2	95.2	92.1	91.7	89.4	88.7
	LTH (Augmix)	95.6	89.4	71.5	80.5	86.0	85.3	94.6	80.9	93.1	93.6	90.5	90.3	92.5	94.8	91.4	91.2	89.5	88.3
	EP (Layerwise Augmix)	94.9	88.4	2.23	83.4	87.3	84.3	93.6	77.8	91.6	92.3	88.3	88.2	90.8	93.9	89.5	90.0	88.9	88.5
	BP (Layerwise Augmix)	94.5	87.8	2.23	82.3	86.3	82.6	93.0	77.4	90.9	91.9	87.6	87.4	90.5	93.5	89.1	89.7	87.8	88.1
	EP (Global Augmix)	94.3	87.8	2.23	83.5	87.1	82.8	92.9	78.1	90.9	91.7	87.4	87.2	89.7	93.0	87.4	89.6	88.6	88.3
	BP (Global Augmix)	93.9	87.5	2.23	82.9	86.6	83.3	92.4	77.8	90.3	91.2	87.0	87.1	89.4	92.7	86.8	89.1	88.4	87.9
	LRR (Gaussian)	93.8	86.4	71.5	91.7	92.2	89.1	87.9	81.8	83.2	86.7	87.5	88.8	79.8	92.4	68.8	87.5	89.4	90.9
	LTH (Gaussian)	93.5	85.8	71.5	91.6	92.0	88.5	87.0	79.0	82.5	86.0	86.7	87.9	80.9	92.1	69.5	87.2	88.4	90.4
	EP (Layerwise Gaussian)	93.0	85.7	2.23	91.0	91.4	88.5	86.6	81.6	81.6	85.7	86.2	88.2	80.8	91.0	71.1	85.9	88.7	89.8
	BP (Layerwise Gaussian)	93.2	85.3	2.23	90.7	91.1	88.2	86.0	80.6	79.9	84.9	86.2	87.6	82.1	91.5	71.3	85.7	87.4	89.5
	BP (Global Gaussian)	92.4	85.1	2.23	90.3	90.8	88.6	85.8	80.3	80.6	84.5	85.2	86.8	81.8	90.0	70.3	85.5	87.5	89.2
	EP (Global Gaussian)	92.4	85.1	2.23	90.4	90.9	88.6	86.2	81.4	81.0	85.2	85.1	87.2	80.4	90.2	68.9	85.5	88.4	89.4
	EP (Global Clean)	93.7	76.7	2.23	64.4	71.6	64.4	82.8	56.8	77.7	78.2	80.4	78.8	87.6	92.0	77.1	84.8	77.6	83.9
	LRR (Clean)	95.6	76.3	71.5	48.2	61.0	55.7	85.2	58.5	81.9	81.5	84.5	80.5	89.6	94.2	79.8	86.6	78.9	81.5
	BP (Global Clean)	93.7	76.1	2.23	61.2	70.1	62.9	82.6	56.6	78.2	79.3	80.5	78.6	87.3	91.7	75.7	84.4	76.6	82.6
	LTH (Clean)	94.9	74.4	71.5	46.2	59.3	51.8	82.9	55.9	78.8	78.9	83.2	79.7	88.8	93.5	78.7	85.7	77.9	80.7
	EP (Layerwise Clean)	94.4	74.4	2.23	50.6	62.0	55.7	82.8	51.1	78.0	78.1	80.9	77.3	88.3	92.9	81.2	84.2	76.6	81.9
	BP (Layerwise Clean)	94.1	74.3	2.23	53.0	64.1	56.2	82.8	50.8	77.4	78.5	80.1	76.7	87.9	92.5	78.2	83.9	75.6	81.2

Table 5: Performance when using ResNet-18 architecture with 80% of weights pruned evaluated on CIFAR-10 and CIFAR-10-C. Note: LTH and LRR model prune rates are 79%.

Model	Noise			Blur			Weather			Digital									
	Clean	Avg. Robust	Memory (Mbit)	gaussian	shot	impulse	defocus	glass	motion	zoom	snow	frost	fog	brightness	contrast	elastic	pixelate	jpeg	
Baseline	Dense (Augmix)	95.5	89.2	358	81.7	85.9	86.7	94.3	80.8	92.4	93.2	90.0	89.7	92.2	94.7	91.0	90.5	88.7	87.7
	Dense (Gaussian)	93.9	85.6	358	91.3	91.8	88.3	85.8	81.0	80.9	84.9	86.4	88.3	81.9	92.3	70.6	86.6	88.1	89.9
	Dense (Clean)	95.1	73.7	358	46.5	59.1	54.0	81.8	55.1	78.1	76.4	82.4	78.2	88.2	93.5	78.2	84.0	76.1	79.3
	LRR (Augmix)	96.3	90.1	35.8	79.2	85.4	89.3	95.3	81.6	93.8	94.4	91.5	91.3	93.3	95.5	92.5	91.8	89.8	88.7
	LTH (Augmix)	95.7	89.4	35.8	79.9	85.5	86.5	94.8	81.1	93.2	93.9	91.0	90.6	92.8	94.9	91.7	91.4	89.9	88.6
	EP (Global Augmix)	94.4	88.0	1.12	83.2	87.1	82.9	93.0	77.6	91.0	92.0	87.7	88.0	90.4	93.4	88.8	89.6	88.9	88.2
	EP (Layerwise Augmix)	94.4	87.9	1.12	83.1	86.5	84.5	93.0	77.6	90.9	91.9	87.7	87.5	90.1	93.3	88.5	89.5	88.1	88.1
	BP (Global Augmix)	94.4	87.8	1.12	83.0	86.9	83.8	92.9	76.6	90.5	91.6	87.6	87.5	89.9	93.2	88.7	89.5	88.1	87.8
	BP (Layerwise Augmix)	93.7	87.1	1.12	81.9	85.8	82.3	92.2	76.8	90.0	91.0	87.0	86.5	89.5	92.5	86.9	89.0	87.2	87.8
	LRR (Gaussian)	94.0	86.4	35.8	91.9	92.5	89.1	88.0	81.3	82.9	86.7	87.8	88.7	80.9	92.3	69.0	87.6	89.6	91.0
	LTH (Gaussian)	93.8	86.0	35.8	91.8	92.2	88.5	87.4	79.2	82.8	86.6	87.0	88.4	81.8	92.4	70.0	87.4	88.4	90.3
	EP (Layerwise Gaussian)	92.8	85.4	1.12	90.6	91.1	88.3	86.2	81.0	80.9	85.2	85.6	87.4	80.9	90.7	71.2	85.6	87.7	89.6
	EP (Global Gaussian)	92.9	85.2	1.12	90.8	91.1	88.7	86.4	80.5	80.8	85.2	85.4	87.0	80.9	90.8	69.8	85.8	87.4	89.4
	BP (Global Gaussian)	92.7	85.0	1.12	90.4	90.9	88.5	85.1	80.2	79.8	83.9	85.5	87.4	81.5	90.4	71.1	85.2	86.6	89.2
	BP (Layerwise Gaussian)	93.0	84.2	1.12	89.9	90.4	87.0	85.2	79.5	79.5	83.8	84.6	87.5	80.9	91.1	69.3	84.5	86.6	88.9
	LRR (Clean)	95.6	76.6	35.8	47.6	60.5	55.2	85.1	61.1	82.0	81.4	84.9	81.2	90.3	94.3	81.4	86.4	79.7	81.3
	EP (Layerwise Clean)	94.1	76.0	1.12	60.7	69.3	62.5	83.5	52.7	77.9	79.1	79.8	78.1	87.5	92.3	78.0	84.2	75.7	82.1
	EP (Global Clean)	93.9	75.6	1.12	55.5	66.1	59.9	84.2	52.3	78.6	80.4	81.1	77.9	88.4	92.4	79.1	84.1	76.7	82.3
	BP (Global Clean)	94.1	75.1	1.12	56.9	66.8	62.0	82.6	54.3	77.2	77.9	80.6	78.5	87.9	92.2	76.9	83.4	74.9	81.3
BP (Layerwise Clean)	93.6	74.6	1.12	54.2	64.7	59.3	83.0	50.8	77.0	78.2	79.5	76.6	87.5	91.9	77.0	83.5	75.0	81.8	
LTH (Clean)	95.2	74.5	35.8	45.5	58.4	53.2	83.5	56.1	79.6	79.9	83.3	79.4	89.1	93.9	78.6	85.6	77.6	80.4	

Table 6: Performance when using ResNet-18 architecture with 90% of weights pruned evaluated on CIFAR-10 and CIFAR-10-C. Note: LTH and LRR model prune rates are 89%.

Model	Noise			Blur			Weather			Digital									
	Clean	Avg. Robust	Memory (Mbit)	gaussian	shot	impulse	defocus	glass	motion	zoom	snow	frost	fog	brightness	contrast	elastic	pixelate	jpeg	
Baseline	Dense (Augmix)	95.5	89.2	358	81.7	85.9	86.7	94.3	80.8	92.4	93.2	90.0	89.7	92.2	94.7	91.0	90.5	88.7	87.7
	Dense (Gaussian)	93.9	85.6	358	91.3	91.8	88.3	85.8	81.0	80.9	84.9	86.4	88.3	81.9	92.3	70.6	86.6	88.1	89.9
	Dense (Clean)	95.1	73.7	358	46.5	59.1	54.0	81.8	55.1	78.1	76.4	82.4	78.2	88.2	93.5	78.2	84.0	76.1	79.3
	LRR (Augmix)	96.1	90.1	17.9	79.2	85.3	89.6	95.2	81.5	93.8	94.3	91.6	91.4	93.3	95.4	92.4	91.8	89.7	88.8
	LTH (Augmix)	95.9	89.5	17.9	78.0	84.5	87.0	94.7	81.1	93.1	93.8	90.9	90.5	92.8	94.9	91.5	91.6	89.3	88.4
	EP (Global Augmix)	94.5	87.8	0.56	82.1	86.5	83.1	93.2	77.1	90.9	92.0	87.8	87.7	90.3	93.3	88.5	89.5	88.1	87.5
	BP (Global Augmix)	94.2	87.5	0.56	82.0	86.1	83.4	92.8	76.5	90.2	91.5	87.2	87.4	89.8	93.0	87.9	89.2	87.5	87.4
	LRR (Gaussian)	94.0	86.5	17.9	91.9	92.3	88.9	87.7	80.4	83.3	86.7	87.7	88.8	81.1	92.6	70.2	87.8	89.2	90.7
	LTH (Gaussian)	93.8	86.0	17.9	91.7	92.1	88.4	87.5	77.6	82.9	86.5	86.7	87.8	82.2	92.3	70.5	87.5	87.6	90.3
	EP (Layerwise Augmix)	93.2	85.7	0.56	81.7	85.1	82.9	91.3	73.5	88.2	89.8	85.6	85.4	88.4	91.8	85.5	87.7	85.4	86.9
	BP (Layerwise Augmix)	92.5	84.7	0.56	80.6	84.2	81.3	90.7	73.0	87.4	89.0	84.1	83.6	87.2	90.9	83.6	86.9	85.4	86.8
	BP (Global Gaussian)	92.5	84.4	0.56	90.1	90.7	88.2	85.2	78.8	79.0	84.0	85.0	86.5	80.7	90.2	69.1	84.9	85.6	89.0
	EP (Global Gaussian)	92.6	84.3	0.56	90.3	90.7	88.2	85.3	78.6	78.9	84.2	85.1	86.6	79.8	90.2	68.0	84.8	85.7	89.0
	EP (Layerwise Gaussian)	91.2	83.9	0.56	88.8	89.6	86.5	85.6	79.5	79.6	84.5	84.2	85.7	79.0	89.2	67.9	84.4	85.8	88.2
	BP (Layerwise Gaussian)	91.4	83.1	0.56	88.6	89.2	85.8	84.8	78.5	79.0	83.4	83.8	85.3	80.9	89.7	67.3	83.6	85.5	87.9
	LRR (Clean)	95.7	75.8	17.9	46.1	59.4	56.4	85.0	58.9	81.1	81.0	84.5	80.3	89.5	94.4	80.9	86.3	79.5	80.7
	LTH (Clean)	95.2	75.1	17.9	48.0	60.8	53.7	83.2	56.0	78.0	78.7	83.4	79.8	88.9	93.9	79.1	85.3	78.3	80.9
	BP (Global Clean)	93.8	73.8	0.56	49.9	61.8	57.2	82.2	51.1	77.0	78.1	79.7	76.8	87.6	92.1	78.4	82.9	74.9	80.7
EP (Layerwise Clean)	92.7	73.4	0.56	56.1	64.9	63.3	82.1	48.6	76.9	77.2	78.1	73.5	86.3	90.9	77.2	82.4	73.8	81.4	
BP (Layerwise Clean)	92.1	73.4	0.56	61.4	69.3	64.1	80.0	51.5	74.6	74.0	77.8	74.5	85.6	90.1	72.7	81.5	72.2	81.5	
EP (Global Clean)	94.0	73.1	0.56	49.3	60.2	57.6	82.0	52.5	75.7	77.6	79.2	75.9	87.0	92.1	74.8	82.9	74.3	80.6	

Table 7: Performance when using ResNet-18 architecture with 95% of weights pruned evaluated on CIFAR-10 and CIFAR-10-C.

CARD-Deck (Agnostic)	Baseline																		
	Model	Clean	Avg. Robust	Memory (Mbit)	Noise			Blur			Weather			Digital					
Dense (Augmix)		95.5	89.2	358	gaussian	shot	impulse	defocus	glass	motion	zoom	snow	frost	fog	brightness	contrast	elastic	pixelate	jpeg
Dense (Gaussian)		93.9	85.6	358															
Dense (Clean)		95.1	73.7	358															
LRR (6)	96.4	91.9	429	88.8	91.5	91.6	95.1	84.7	93.3	94.3	92.2	92.3	92.3	95.5	90.5	92.6	91.6	92.1	
LRR (4)	96.3	91.7	286	87.1	90.5	91.0	95.1	84.6	93.4	94.4	92.2	92.3	92.6	95.5	89.6	92.1	90.9	91.6	
LTH (6)	96.1	91.2	429	88.8	91.5	89.8	94.4	83.6	92.5	93.6	91.4	91.6	91.6	95.1	90.3	92.0	90.7	91.1	
LTH (4)	96.0	91.0	286	87.7	90.6	88.9	94.5	83.4	92.7	93.8	91.4	91.5	91.9	95.0	90.3	92.0	90.7	91.1	
LRR (2)	96.0	89.7	143	77.9	84.3	87.1	95.1	81.3	93.6	94.1	91.4	90.8	93.1	95.2	91.9	91.5	89.2	88.7	
LTH (2)	95.5	89.4	143	80.5	86.0	84.9	94.6	80.9	93.0	93.6	90.5	90.2	92.4	94.8	91.4	91.1	89.5	87.9	
BP (6)	94.3	89.0	13.4	89.7	91.2	88.9	91.9	82.2	89.1	90.6	88.3	89.2	88.2	93.0	83.1	89.8	89.4	90.4	
BP (4)	94.3	88.8	8.94	88.9	90.6	88.1	92.0	81.4	89.4	90.8	88.1	88.9	88.4	92.9	83.9	89.7	88.9	90.1	
BP (2)	93.8	87.5	4.47	82.9	86.6	83.3	92.4	77.8	90.3	91.2	87.0	87.1	89.1	92.7	86.8	89.1	87.7	87.9	

Table 8: Performance of data-agnostic CARD-Deck ensembles composed of 80% sparse ResNet-18 CARDs on individual CIFAR-10-C corruptions. For each corruption, entry is average over severity levels 1 through 5.

CARD-Deck (Agnostic)	Baseline																		
	Model	Clean	Avg. Robust	Memory (Mbit)	Noise			Blur			Weather			Digital					
	Dense (Augmix)	95.5	89.2	358	gaussian	shot	impulse	defocus	glass	motion	zoom	snow	frost	fog	brightness	contrast	elastic	pixelate	jpeg
	Dense (Gaussian)	93.9	85.6	358															
	Dense (Clean)	95.1	73.7	358															
	LRR (6)	96.4	92.0	215	89.4	91.9	91.9	95.0	85.0	93.3	94.2	92.2	92.4	92.2	95.6	90.5	92.6	91.5	92.1
	LRR (4)	96.4	91.7	143	87.6	90.8	91.2	95.1	84.4	93.5	94.3	92.1	92.1	92.6	95.5	91.1	92.3	91.1	91.6
	LTH (6)	96.2	91.3	215	88.9	91.6	89.8	94.4	83.7	92.5	93.7	91.6	91.8	91.7	95.2	89.8	92.1	91.0	91.7
	LTH (4)	95.9	91.0	143	87.4	90.5	88.3	94.5	83.1	92.9	93.8	91.6	91.6	92.1	95.2	90.4	92.0	90.7	91.1
	LRR (2)	96.3	89.8	71.5	77.7	84.3	87.2	95.3	81.4	93.8	94.4	91.4	91.0	93.1	95.5	91.9	91.7	89.8	88.7
	LTH (2)	95.7	89.4	71.5	79.9	85.5	83.2	94.7	81.1	93.2	93.9	90.8	90.6	92.5	94.9	91.7	91.2	89.9	87.8
	BP (6)	94.5	89.4	6.70	89.9	91.5	89.1	92.1	81.9	89.3	91.1	89.0	89.7	88.8	93.5	85.1	90.0	89.5	90.7
	BP (4)	94.6	89.2	4.47	88.8	90.7	88.2	92.3	81.0	89.7	91.2	88.7	89.4	89.2	93.4	85.7	90.0	89.3	90.2
	BP (2)	94.0	87.4	2.23	82.0	86.3	82.7	92.5	76.5	90.3	91.5	87.3	86.8	89.7	92.8	87.8	89.5	88.1	87.6

Table 9: Accuracy of data-agnostic CARD-Deck ensembles composed of 90% sparse ResNet-18 CARDs on individual CIFAR-10-C corruptions. For each corruption, entry is average over severity levels 1 through 5.

CARD-Deck (Agnostic)	Baseline																		
	Model	Clean	Avg. Robust	Memory (Mbit)	Noise			Blur			Weather			Digital					
LRR (6)					gaussian	shot	impulse	defocus	glass	motion	zoom	snow	frost	fog	brightness	contrast	elastic	pixelate	jpeg
LRR (4)																			
LTH (6)																			
LTH (4)																			
LRR (2)																			
BP (6)																			
LTH (2)																			
BP (4)																			
BP (2)																			

Table 10: Accuracy of data-agnostic CARD-Deck ensembles composed of 95% sparse ResNet-18 CARds on individual CIFAR-10-C corruptions. For each corruption, entry is average over severity levels 1 through 5.

		Baseline			ResNet-18					
		Dense			FT			GMP		
		-			Global			Global		
		Augmix	Clean	Gauss.	Augmix	Clean	Gauss.	Augmix	Clean	Gauss.
80%	Clean Acc.	95.5	95.1	93.9	95.6	94.6	94.1	95.1	94.3	93.4
	Robust Acc.	89.2	73.7	85.6	88.7	73.6	84.5	88.2	73	84.5
	Memory (Mbit)	358	358	358	143	286	429	143	286	429
90%	Clean Acc.	95.5	95.1	93.9	94.7	94.1	93.1	94.8	94	93.4
	Robust Acc.	89.2	73.7	85.6	87.2	71.5	83.5	87.7	72.9	83.7
	Memory (Mbit)	358	358	358	71.5	143	215	71.5	143	215
95%	Clean Acc.	95.5	95.1	93.9	93.8	93.4	92.2	94.6	93.9	92.9
	Robust Acc.	89.2	73.7	85.6	85.4	68	81.1	87.2	73	83.7
	Memory (Mbit)	358	358	358	35.8	71.5	107	35.8	71.5	107

Table 11: Performance comparison between dense baselines and ResNet-18 models pruned using fine-tuning (FT) and gradual magnitude pruning (GMP). Clean and Robust Acc. refer to accuracy on CIFAR-10 and CIFAR-10-C, respectively.

		Baseline			CARD																	
		Dense			Edgepopup						LRR			LTH			Biprop					
		-			Layerwise			Global			Global			Global			Layerwise			Global		
		Augmix	Clean	Gauss.	Augmix	Clean	Gauss.	Augmix	Clean	Gauss.	Augmix	Clean	Gauss.	Augmix	Clean	Gauss.	Augmix	Clean	Gaussian	Augmix	Clean	Gauss.
90%	Clean Acc.	95.9	95.4	93.8	94.2	94.2	93	94.4	94	92.9	96.4	95.4	94.2	96.2	96	94	94.2	94	92.8	93.7	93.6	92.4
	Robust Acc.	88.2	71.2	84.3	86.5	72	83	86.7	72.1	83	89.4	71.8	85.5	88.8	73.1	84.3	86.2	71.5	83.1	86	71.5	82.7
	Memory (Mbit)	153	153	153	0.48	0.48	0.48	0.48	0.48	0.48	15.28	15.28	15.28	15.28	15.28	15.28	0.48	0.48	0.48	0.48	0.48	0.48
95%	Clean Acc.	95.9	95.4	93.8	93.7	93.7	93	91.7	91.5	90.4	96.3	95.5	94.3	96.1	95.8	93.9	93.6	93.5	92.4	90.9	91.2	90.2
	Robust Acc.	88.2	71.2	84.3	85.8	69.9	82.3	82.8	69	80.3	89.3	71.3	85.6	88.4	72.8	84.6	85.1	70.3	81.8	82.4	70.4	80.2
	Memory (Mbit)	153	153	153	0.24	0.24	0.24	0.24	0.24	0.24	7.64	7.64	7.64	7.64	7.64	7.64	0.24	0.24	0.24	0.24	0.24	0.24

Table 12: Performance comparison between dense baselines and CARDs for ResNeXt-29. Clean and Robust Acc. refer to accuracy on CIFAR-10 and CIFAR-10-C, respectively.

		Baseline									CARD											
		Dense			Edgepopup						LRR			LTH			Biprop					
		-			Layerwise			Global			Global			Global			Layerwise			Global		
		Augmix	Clean	Gauss.	Augmix	Clean	Gauss.	Augmix	Clean	Gauss.	Augmix	Clean	Gauss.	Augmix	Clean	Gauss.	Augmix	Clean	Gaussian	Augmix	Clean	Gauss.
90%	Clean Acc.	95.9	95.1	93.6	94.8	94.4	93.3	95.4	95	94	96.6	95.6	94.7	96.3	96	94.3	94.7	94.4	93	94.9	94.7	93.2
	Robust Acc.	88.9	74.4	85.2	88	75.8	84.8	89.1	76.6	86.3	90.5	77.5	87	90	76.9	86.2	87.9	74.6	85.1	88.6	75.6	85.6
	Memory (Mbit)	753	753	753	2.35	2.35	2.35	2.35	2.35	2.35	75.27	75.27	75.27	75.27	75.27	75.27	2.35	2.35	2.35	2.35	2.35	2.35
95%	Clean Acc.	95.9	95.1	93.6	92.4	93.6	92.2	95	94.8	93.4	96.5	95.7	94.9	96.3	95.9	94.3	94.6	94.6	93.2	94.4	93.9	92.6
	Robust Acc.	88.9	74.4	85.2	79.2	70.9	82.6	88.9	76.6	85.9	90.6	77.6	87	89.9	76.2	86.3	87.4	73.9	84.8	87.6	74.4	84.6
	Memory (Mbit)	753	753	753	1.18	1.18	1.18	1.18	1.18	1.18	37.63	37.63	37.63	37.63	37.63	37.63	1.18	1.18	1.18	1.18	1.18	1.18

Table 13: Performance comparison between dense baselines and CARDs for ResNet-50. Clean and Robust Acc. refer to accuracy on CIFAR-10 and CIFAR-10-C, respectively.

		Baseline			CARD																			
		Dense																						
					Edgepopup						LRR			LTH			Biprop							
					Layerwise			Global			Global			Global			Layerwise			Global				
		Augmix	Clean	Gauss.	Augmix	Clean	Gauss.	Augmix	Clean	Gauss.	Augmix	Clean	Gauss.	Augmix	Clean	Gauss.	Augmix	Clean	Gaussian	Augmix	Clean	Gauss.		
90%	Clean Acc.	95.6	95.2	93.3	94.8	94.2	92.4	95.0	94.7	92.8	96.3	95.9	94	96.1	95.6	94.1	94.5	94.4	92.7	94.6	94.1	92.6		
	Robust Acc.	89.3	74.6	85.7	88.6	78.2	85.5	88.8	76.5	85.7	90.5	76.8	86.6	89.8	75.5	86.5	88.4	77.4	85.6	88.3	75.7	85.3		
	Memory (Mbit)	1429	1429	1429	4.47	4.47	4.47	4.47	4.47	4.47	142.9	142.9	142.9	142.9	142.9	142.9	4.47	4.47	4.47	4.47	4.47	4.47		
95%	Clean Acc.	95.6	95.2	93.3	94.9	94.4	92.8	94.2	93.8	92.1	96.4	95.8	94.2	96.1	95.8	94.3	94.7	94.3	92.7	93.6	93.3	91.5		
	Robust Acc.	89.3	74.6	85.7	88.7	75.6	85.2	87.6	75.9	85.0	90.8	77.1	87.0	90.0	76.2	86.6	88.6	76.1	84.9	87.3	76.0	84.6		
	Memory (Mbit)	1429	1429	1429	2.23	2.23	2.23	2.23	2.23	2.23	71.46	71.46	71.46	71.46	71.46	71.46	2.23	2.23	2.23	2.23	2.23	2.23		

Table 14: Performance comparison between dense baselines and CARDs for WideResNet-18 (2x). Clean and Robust Acc. refer to accuracy on CIFAR-10 and CIFAR-10-C, respectively.

		CARD-Deck (Agnostic/Adaptive)					
		Biprop (Layerwise)			Edgepopup (Layerwise)		
		2	4	6	2	4	6
90%	Clean Acc.	92.3/ 93.0	94.0/ 94.5	94.8/ 95.1	92.6/ 93.3	94.3/ 95.0	95.2/ 95.4
	Robust Acc.	85.2/ 86.2	88.4/ 89.8	89.9/ 90.5	85.3/ 86.6	89.0/ 90.4	90.6/ 91.0
	Memory (Mbit)	8.93	17.86	26.79	8.93	17.86	26.79
95%	Clean Acc.	91.4/ 92.0	93.3/ 93.6	94.0/ 94.1	92.1/ 92.2	93.8/ 94.1	94.7/ 94.8
	Robust Acc.	84.6/ 85.2	87.4/ 88.7	88.8/ 89.3	85.0/ 85.9	88.1/ 89.3	89.7/ 90.0
	Memory (Mbit)	4.46	8.93	13.39	4.46	8.93	13.39

Table 15: Performance of additional domain-agnostic and domain-adaptive CARD-Decks containing CARDs using WideResNet-18 architecture.

Augmentation	Noise			Blur				Weather				Digital			
	gaussian	shot	impulse	defocus	glass	motion	zoom	snow	frost	fog	brightness	contrast	elastic	pixelate	jpeg
Augmix	0	3.2	0	89	0	100	96.2	100	38.6	100	99.8	100	98.2	99.6	100
Gaussian	100	96.8	100	11	100	0	3.8	0	61.4	0	0.2	0	1.8	0.4	0

Table 16: **Gating Function Selection by Corruption Type on CIFAR-10-C:** The CARD-Decks make use of models trained on Augmix and Gaussian augmented datasets. Here we provide the percentage of CIFAR-10-C test data that was gated to the Augmix and Gaussian models in the CARD-Deck based on the type of corruption. For each corruption type, the bold number indicates which CARD achieves higher performance (on average) on that corruption. This highlights that our spectral similarity based gating function typically selects the best performing model. Note that for impulse and glass corruptions, the best performing models vary between those trained on Augmix and Gaussian corruptions based on the sparsity level of the model. For each corruption type, the percentage in the table gated to each augmentation method is an average over the gating percentages on CIFAR-10-C corruption severity levels 1 through 5.